Archives of Biochemistry and Biophysics 717 (2022) 109125

Contents lists available at ScienceDirect

Archives of Biochemistry and Biophysics

journal homepage: www.elsevier.com/locate/yabbi

Biochemical and biophysical characterization of PADI4 supports its involvement in cancer

José L. Neira [a,b,*], Salomé Araujo-Abad [a,c], Ana Cámara-Artigas [d], Bruno Rizzuti [b,e], Olga Abian [b,f,g,h], Ana Marcela Giudici [a], Adrian Velazquez-Campoy [b,f,g,h], Camino de Juan Romero [a,i,**]

[a] IDIBE, Universidad Miguel Hernández, 03202, Elche, (Alicante), Spain
[b] Instituto de Biocomputación y Física de Sistemas Complejos, Universidad de Zaragoza, 50009, Zaragoza, Spain
[c] Centro de Biotecnología, Universidad Nacional de Loja, Avda. Pio Jaramillo Alvarado s/n, 110111, Loja, Ecuador
[d] Departamento de Química y Física, Research Center CIAIMBITAL, Universidad de Almería, CeiA3, 04120, Almería, Spain
[e] CNR-NANOTEC, SS Rende (CS), Department of Physics, University of Calabria, 87036, Rende, Italy
[f] Instituto de Investigación Sanitaria Aragón (IIS Aragón), Zaragoza, Spain
[g] Centro de Investigación Biomédica en Red en el Área Temática de Enfermedades Hepáticas y Digestivas (CIBERehd), Madrid, Spain
[h] Departamento de Bioquímica y Biología Molecular y Celular, Universidad de Zaragoza, 50009, Zaragoza, Spain
[i] Unidad de Investigación, Fundación para el Fomento de la Investigación Sanitaria y Biomédica de la Comunidad Valenciana (FISABIO), Hospital General Universitario de Elche, Camí de l'Almazara 11, 03203, Elche, (Alicante), Spain

ARTICLE INFO

Keywords:
Cancer
Circular dichroism
Calorimetry
Fluorescence
Protein stability
Western blot

ABSTRACT

PADI4 (protein-arginine deiminase, also known as protein L-arginine iminohydrolase) is one of the human isoforms of a family of Ca^{2+}-dependent proteins catalyzing the conversion of arginine to citrulline. Although the consequences of this process, known as citrullination, are not fully understood, all PADIs have been suggested to play essential roles in development and cell differentiation. They have been found in a wide range of cells and tissues and, among them, PADI4 is present in macrophages, monocytes, granulocytes and cancer cells. In this work, we focused on the biophysical features of PADI4 and, more importantly, how its expression was altered in cancer cells. Firstly, we described the different expression patterns of PADI4 in various cancer cell lines and its colocalization with the tumor-related protein p53. Secondly, we carried out a biophysical characterization of PADI4, by using a combination of biophysical techniques and *in silico* molecular dynamics simulations. Our biochemical results suggest the presence of several forms of PADI4 with different subcellular localizations, depending on the cancer cell line. Furthermore, PADI4 could have a major role in tumorigenesis by regulating p53 expression in certain cancer cell lines. On the other hand, the native structure of PADI4 was strongly pH-dependent both in the absence or presence of Ca^{2+}, and showed two pH-titrations at basic and acidic pH values. Thus, there was a narrow pH range (from 6.5 to 8.0) where the protein was dimeric and had a native structure, supporting its role in histones citrullination. Thermal denaturations were always two-state, but guanidinium-induced ones showed that PADI4 unfolded through at least one intermediate. Our simulation results suggest that the thermal melting of PADI4 structure was rather homogenous throughout its sequence. The overall results are discussed in terms of the functional role of PADI4 in the development of cancer.

1. Introduction

Citrullination, or deamination, is a post-translational modification (PTM) catalyzed by peptidyl-arginine deiminases also known as L-arginine iminohydrolases (EC 3.5.3.15, PADIs). Although the full consequences of the modification of the positive charge of the guanidino group of arginine to the neutral ureido group of citrulline are unknown, it is thought that such PTM induces local protein unfolding, impairing the formation of functional tertiary structures [1,2]. PADIs have key

* Corresponding author. IDIBE, Edificio Torregaitán, Universidad Miguel Hernández, Avda. del Ferrocarril s/n, 03202, Elche, (Alicante), Spain.
** Corresponding author. Unidad de Investigación, Fundación para el Fomento de la Investigación Sanitaria y Biomédica de la Comunidad Valenciana (FISABIO), Hospital General Universitario de Elche, Camí de l'Almazara 11, 03203, Elche, (Alicante), Spain.
E-mail addresses: jlneira@umh.es (J.L. Neira), m.juan@umh.es (C. de Juan Romero).

https://doi.org/10.1016/j.abb.2022.109125
Received 21 December 2021; Received in revised form 14 January 2022; Accepted 17 January 2022
Available online 23 January 2022

roles in nerve growth, onset of inflammation states, embryonic development, tissue aging, epithelial terminal differentiation, trauma cancer cell lines, suggesting that PADI4 could have diverse functional roles depending on the tumor type. Its conformational features and

Abbreviations

ANS	1-anilino-8-naphtalene sulfonate
AUC	analytical ultracentrifugation
BSA	bovine serum albumin
CD	circular dichroism
COAD	colon adenocarcinoma
DAPI	4′, 6′ Diamidin-2-phenylindol
DLS	dynamic light scattering
DSC	differential scanning calorimetry
DSF	differential scanning fluorimetry
FBS	foetal bovine serum
GBM	glioblastoma
GdmCl	guanidinium hydrochloride
IPTG	isopropyl-β-D-1-tiogalactopyranoside
LB	Luria Bertani
MD	molecular dynamics
NLS	nuclear localization signal
PAAD	pancreatic adenocarcinoma
PADI	peptidyl-arginine deiminase
PBS	phosphate buffer solution
PDB	Protein Data Bank
SDS-PAGE	sodium dodecyl sulphate polyacrylamide gel electrophoresis
PTM	protein translational modification
RMSF	root mean square fluctuations
TCEP	Tris(2-carboxyethyl)phosphine
UV	ultraviolet;
WB	western blot

apoptosis and transcriptional regulation of gene expression and regulation [3–10]. Furthermore, several human diseases such as Alzheimer's disease, rheumatoid arthritis, multiple sclerosis, psoriasis and different types of cancers are associated with the presence of PADIs and their citrullinated targets [9,11–13].

To date, five human genes encoding PADI proteins have been found, PADI1, PADI2, PADI3, PADI4 and PADI6 [14–20]. Each enzyme type has a tissue-specific expression, including the uterus and epidermis (PADI1); brain, secretory glands, inflammatory cells, and several cancer cell lines (PADI2); hair follicles and keratinocytes (PADI3); cancer cells, macrophages, monocytes and granulocytes (PADI4); and embryos and oocytes during embryonic development (PADI6), although this latter isoform is a pseudo-enzyme with no detectable catalytic activity. PADI3 displays the highest specificity for synthetic and natural substrates among all the PADIs, and it also modulates cell growth by affecting apoptosis-induced factor-mediated cell death [21,22]. Apoptosis enhanced through the mitochondrial pathway seems to be associated with an increase of enzyme activity of some PADI4 mutants [23]. Furthermore, PADI4 is involved in p53 gene expression, as well as the expression of other p53 target-genes [24,25]. Thus, PADI4 functions as a p53 co-repressor, and therefore, inhibitors of this enzyme could be considered potential treatments of cancer.

All PADIs are found in the cytoplasm, except PADI4, which has been detected in both the cytoplasm and the nucleus, and PADI2, which is also found in the nucleus under some stress conditions [2,26,27]. Moreover, all PADIs are Ca^{2+}-dependent enzymes, as PADI-driven citrullination requires supraphysiological levels of such cation [2,11]. In fact, PADIs are inactive at normal physiological conditions when Ca^{2+} concentration is low, and their activity is triggered by the influx of extracellular calcium, or its release from intracellular calcium stores [11].

PADI4 can convert Arg and monomethyl-Arg to citrulline, thereby regulating histone arginine-methylation catalyzed by members of the protein Arg methyltransferase family [8,10,28]. This PADI4-mediated demethylimination and citrullination of histones have been found to play a role in transcriptional repression of nuclear receptor target genes [3]. The involvement of PADI4 in several diseases, and the fact that is also found in the nucleus where it interacts with histones, have prompted us to study its presence in different cancer cells, and to elucidate its conformational features at different pH values, its stability in the absence and in the presence of Ca^{2+} in solution, and its unfolding properties.

This work revealed that PADI4 expression varied among different stability were studied by using several biophysical and biochemical techniques, namely fluorescence and circular dichroism (CD) spectroscopic techniques, dynamic light scattering (DLS), differential scanning calorimetry (DSC), differential scanning fluorimetry (DSF) and molecular dynamics (MD) simulations. Our results showed that the protein exhibited a native structure in a narrow pH range (pH 6.5 to 8.0), where it was a dimer, either in the presence or in the absence of Ca^{2+}. Within that pH range, PADI4 had an apparent thermal denaturation midpoint of ~55 °C, as judged by thermal denaturations followed by intrinsic and extrinsic fluorescence, far-UV CD, DSF, and DSC; such value is not very high, and might facilitate protein-protein interactions with other partners by promoting PADI4 flexibility. The MD simulations results also indicated an overall flexibility of the protein that appeared to drive a rather homogeneous loss of structure throughout its sequence during the thermal denaturation. In the presence of Ca^{2+}, the shapes of the thermal and heat denaturation calorimetric curves were modified; thus, the interaction with Ca^{2+} can provide another layer for PADI4 function regulation. On the other hand, chemical unfolding occurred through at least an intermediate unfolding species, at variance with the thermal unfolding process.

2. Materials and methods

2.1. Materials

Kanamycin and isopropyl-β-D-1-tiogalactopyranoside (IPTG) were obtained from Apollo Scientific (Stockport, UK). Imidazole, Trizma base, 8-anilino-naphtalene-1-sulfonic acid ammonium salt (ANS) and His-Select HF nickel resin were from Sigma-Aldrich (Madrid, Spain). Triton X-100, TCEP (tris(2-carboxyethyl) phosphine) and protein marker (PAGEmark Tricolor) were from VWR (Barcelona, Spain). Ultrapure guanidinium hydrochloride (GdmCl) and urea were from Pierce (Madison, Wisconsin, USA). Amicon centrifugal devices with a cut-off molecular weight of 30 and 50 kDa were from Millipore (Barcelona, Spain). The rest of the materials used were of analytical grade. Water was deionized and purified on a Millipore system.

2.2. Protein expression and purification

The codon-optimized, N-terminal His-tagged PADI4 inserted in the vector pHTP1 (with kanamycin resistance) was synthesized and produced by NZytech (Lisbon, Portugal). Expression of PADI4 was carried out in *E. coli* BL21 (DE3) strain. The protein was expressed with a final

amount of 0.8 mM of IPTG, when the absorbance at 600 nm of 1 L of LB medium reached a value in the range 0.8–1.0. After induction, cells were grown overnight at 30 °C. They were subsequently harvested by centrifugation at 5 °C for 15 min at 10,000 rpm in a JA-10 rotor (using a Beckman Coulter Avanti J26-XP Centrifuge). The cell pellet was resuspended in washing buffer (20 mM sodium phosphate (pH 8.0) with 300 mM NaCl, containing 20 mM imidazole) with an additional tablet of SIGMAFAST protease inhibitor cocktail EDTA-free, and DNase with a final concentration of 2 mg/L of LB medium (Sigma-Aldrich, Madrid, Spain). Cells were disrupted while cooled on ice by using a Branson sonicator for 10 periods (amplitude 25% of the maximum power) of 60 s, alternated with periods of 60 s on ice. The resulting lysate was centrifuged at 5 °C for 30 min at 17,000 rpm in a JA-20 rotor (Beckman Coulter, Barcelona, Spain) by using the same centrifuge as in the harvesting step. The rest of the purification protocol was the same previously described to purify other PADI isoforms [29–31], but in our case we used TCEP as a redox agent and the final concentration of glycerol was 5%. Briefly, after elution from the Ni-resin the protein was exchanged back (by using Amicon centrifugal devices with a cut-off of 30 K) to 50 mM Tris buffer (pH 7.5), 5 mM TCEP, 10 mM EDTA, 150 mM NaCl and 5% glycerol (Elution buffer). The resulting solution was loaded in a Hi-Trap Q HP column (5 mL) (GE Healthcare, Barcelona, Spain) and eluted with a gradient from the above buffer to the same buffer modified by adding 1 M NaCl in 1 h with a flow rate of 1 mL/min. The protein eluted in the range 20%–30% of 1 M NaCl. After that, the protein was also exchanged back to the Elution buffer and loaded in a gel filtration column Superdex 200 (HiLoad 16/60) (GE Healthcare), which had been previously equilibrated in the Elution buffer. Both columns were connected to an AKTA FPLC machine and the protein was detected by following the absorbance of the eluting solution at 280 nm. After expression and purification of several litres of media, we could also confirm that, after elution from the resin, by using solely an Amicon 50 K, and exchanging to Elution buffer, the protein was pure enough to carry out the biophysical studies. Protein was stored in the Elution buffer, after being flash frozen, at −20 °C until use. For the experiments in the presence of Ca^{2+}, the protein, once purified, was exchanged from the elution buffer containing 10 mM EDTA to one containing 10 mM Ca^{2+}. The protein maintained its His-tag all along the purification process, and was used as such in the experiments.

Protein concentration was determined from the absorbance at 280 nm of the 13 tyrosine and 10 tryptophan residues of each PADI4 monomer [32].

2.3. Cell lines

The human colon carcinoma (HT-29) and pancreatic adenocarcinoma (RWP-1) cell lines, were donated by Instituto Municipal de Investigaciones Médicas (IMIM, Barcelona, Spain) [33]. Isolation of primary human glioblastoma cell line (GB-39) was performed from surgical wash, as reported previously [34]. HT-29 and RWP1 cell lines were cultured in Dubelcco's Modified Eagle's Medium: High Glucose (DEMEM-HG) (Biowest, MO, USA) whereas glioblastoma (GBM) cells were cultured in Dubelcco's Modified Eagle's Medium: Nutrient Mixture F-12 (DMEM F-12) (Biowest, MO, USA). Both culture media, were supplemented with 10% (v/v) heat-inactivated foetal bovine serum (FBS) (Biowest, MO, USA) and 1% (v/v) penicillin/streptomycin mixture (Biowest, MO, USA). Cells were incubated at 37 °C in a humidified 5% CO_2 atmosphere.

2.4. Western Blot (WB)

All cell lysates were analysed for total protein concentration using the BCA protein assay kit (Pierce™, Thermo Scientific, Madrid, Spain); an amount of 20 μg of total protein was solubilized with loading buffer (4x) (2-mercaptoethanol + NuPage; (1:5)) and heated at 95 °C for 5 min. Then, they were separated by using 10% SDS-PAGE, and transferred to a nitrocellulose membrane (Bio-Rad Laboratories Inc, California, USA). Following standard protocols, membranes were incubated overnight at 4 °C with primary antibodies: anti-PADI4 (rabbit,1:2500, Invitrogen, Barcelona, Spain), anti-p53 (mouse,1:500, Calbiochem, Madrid, Spain) and anti-HSP90-B1 (rabbit,1:4000, CUSABIO, Houston, USA) followed by 1 h incubation at room temperature with ECL™ anti-mouse IgG and ECL™ anti-rabbit IgG, Horseradish Peroxidase linker (GE Healthcare, UK). The membranes were visualized with ECL™ Prime Western blotting detection reagent (Amersham™, Barcelona, Spain) in a ChemiDoc Bio-Rad (Bio-Rad) instrument.

2.5. Immunofluorescence

Cell cultures were fixed with formaldehyde for 20 min and then washed with phosphate buffer solution (PBS) (1x). Coverslips were blocked with 10% horse serum, 2% bovine serum albumin (BSA), 0.25% Triton in PBS for 1.5 h prior to staining. Primary antibodies anti-PADI4 (rabbit,1:300, Invitrogen) and anti-p53 (mouse,1:300, Calbiochem) were prepared in blocking solution and applied to samples to incubate overnight at 4 °C. Then, primary antibodies were washed with PBS (1x) and fluorescent secondary antibodies were applied (1:1000, Invitrogen) and incubated for 1.5 h at room temperature. In order to visualize the nuclei, samples were incubated for 5 min in 0.1 μg/mL DAPI (4′.6-Diamidin-2-phenylindol, Sigma). Coverslips were mounted in Vectashield H-1000 (Vector Laboratories, CA, USA) and analysed using Zeiss Axioscope 5 microscope with the LED light source Colibri 3.

2.6. Fluorescence

(a) Steady-state fluorescence

Fluorescence spectra were collected on a Cary Eclipse Varian spectrofluorometer (Agilent, CA, USA), interfaced with a Peltier unit. Unless it is stated otherwise, all experiments were carried out at 25 °C. Following the standard protocols used in our laboratories, the samples were prepared the day before and left overnight at 5 °C; before experiments, samples were left for 1 h at 25 °C. A 1-cm-pathlength quartz cell (Hellma, Kruibeke, Belgium) was used. Protein concentration was 1.5 μM, in protomer units. A control experiment to follow GdmCl-denaturation by measuring intrinsic fluorescence was carried out by using a final protein concentration of 10.5 μM, in protomer units. The pathlength of the cell was 1 cm.

For the pH-denaturation experiments either in the presence of Ca^{2+} (10 mM) or in its absence (10 mM EDTA), protein samples were excited at either 280 or 295 nm in the pH range from 2.0 to 12.0. Slit widths were 5 nm. The final buffer concentration was 50 mM in all cases containing 5% glycerol and 5 mM TCEP, and the corresponding salts and acids used were: pH 2.0–3.0, phosphoric acid; pH 3.0–4.0, formic acid; pH 4.0–5.5, acetic acid; pH 6.0–7.0, NaH_2PO_4; pH 7.5–9.0, Tris acid; pH 9.5–11.0, Na_2CO_3; pH 11.5–13.0, Na_3PO_4. Appropriate blank corrections were made in all spectra. The pH of each sample was measured after completion of experiments with an ultra-thin Aldrich (Madrid, Spain) electrode in a Radiometer (Copenhagen, Denmark) pH-meter.

Chemical-denaturations at pH 7.5 (in 50 mM Tris buffer, with 5% glycerol and 5 mM TCEP) either followed by intrinsic or ANS (see below) fluorescence, and far-UV CD experiments (see below) were carried out by dilution of the proper amount of a 7 M GdmCl stock solution. Experiments were carried out either in the presence of Ca^{2+} (10 mM, final concentration) or in its absence (10 mM EDTA, final concentration). Also, urea denaturations were followed at the same pH, but the stock solution of denaturant agent used to prepare the samples was 8 M. In all cases, spectra from blank solutions were subtracted from the corresponding spectra in the presence of the protein. The GdmCl or urea concentrations in the stock solutions were quantified by using refractive index measurements [35]. Both the chemical- and pH-denaturations were repeated at least three times with different samples. Variations

by using the same voltage in the fluorescence photomultiplier from experiments repeated day to day were 2–5%.

(b) *Thermal-denaturations*

Experiments were performed at constant heating rates of 60 °C h^{-1} with an average time of 1 s. Thermal scans were collected at 315, 330 and 350 nm after excitation at either 280 or 295 nm, typically from 25 to 80 °C. The rest of the experimental set-up was the same described above. Thermal denaturations were irreversible; irreversibility was tested by acquiring steady-state spectra of thermally denatured proteins, and by comparing their shape and intensity with those of the spectra acquired before heating. The apparent thermal denaturation midpoint, T_m, was estimated from a two-state equilibrium equation taking into account the concentration-dependence of the unfolding (see below).

(c) *ANS binding*

The excitation wavelength was 370 nm, and emission was measured from 400 to 600 nm at 25 °C. Slit widths were 5 nm for both excitation and emission. ANS stock solution (10 mM) was prepared in water and diluted to yield a final concentration of 100 μM in each sample, with a final protein protomer concentration of 1.5 μM (both in the pH- or GdmCl-denaturation experiments at pH 7.5). The same set of buffers and their concentrations used in the steady-state intrinsic fluorescence experiments (see above) were utilized for the pH-denaturations followed by ANS. Experiments were carried out either in the presence of Ca^{2+} (10 mM, final concentration) or in its absence (10 mM EDTA, final concentration). Spectra from blank solutions were subtracted from the corresponding spectra. In the pH-denaturations, the pH of each sample was measured after completion of titration with an ultra-thin Aldrich electrode in a Radiometer pH-meter.

We also used ANS to follow thermal denaturations, as it can provide information on how the different solvent-exposed hydrophobic patches change their environment upon heating [36]. The experimental set-up in these denaturations was the same used for measuring the intrinsic fluorescence of the protein, except for the excitation (370 nm) and emission (480 nm) wavelengths. Thermal denaturations were always irreversible.

(d) *Differential scanning fluorimetry (DSF)*

Experiments were acquired in a Mx3005p real-time qPCR (Agilent, Madrid, Spain) using SYPRO Orange as an extrinsic fluorescence probe, and we measured its fluorescence intensity as a function of temperature. As the protein unfolds, SYPRO Orange binds to hydrophobic patches and its quantum yield increases, indirectly reporting about the protein unfolding process. We used 50 μL of total volume with PADI4 at a concentration of 4 μM (in protomer units) and a concentration of dye of 5 x, in 50 mM Tris buffer (pH 7.5), 5 mM TCEP and 5% glycerol. We are fully aware that the pK_a of Tris is temperature-dependent, but we have preferred to use this buffer as it is the one employed at the high protein concentrations of DSC experiments (see below). Furthermore, the use of phosphate buffer could lead to precipitation of calcium in the experiments in the presence of the cation. DSF provides a signal reflecting the global unfolding of the protein, but it may overlook some unfolding steps, if present; therefore, it is usually employed as a semi-quantitative technique, mainly aimed at identifying potential ligands for a given protein target [37].

The mathematical treatment of the experimental data may rely on a simple estimation of the unfolding temperature, T_m, through identification of the temperature for maximal slope of the fluorescence signal, or the calculation of the unfolded fraction, F_U, through a well-known normalization procedure:

$$F_U(T) = \frac{S(T) - S_N(T)}{S_U(T) - S_N(T)} \quad (1)$$

where $S(T)$ is the measured signal at any temperature T, and $S_N(T)$ and $S_U(T)$ are the intrinsic signals corresponding to the native and unfolded protein states, usually considered to be linear functions of the temperature. We have used Eq. (1) to normalize the experimental data obtained by DSF, and the analyses of the thermal denaturation curves were carried out by using the equations described below (Eq. (9)), taking into account the concentration-dependence of the unfolding. A further calculation allows the estimation of the unfolding enthalpy from the temperature derivative of the unfolded fraction at T_m:

$$\Delta H(T_m) = 4RT_m^2 \left(\frac{\partial F_U(T)}{\partial T} \right)_{T=T_m} \quad (2)$$

2.7. Circular dichroism (CD)

The steady-state CD spectra were collected on a Jasco J810 spectropolarimeter (Jasco, Tokyo, Japan) with a thermostated cell holder, and interfaced with a Peltier unit at 25 °C. The instrument was periodically calibrated with (+)-10-camphorsulphonic acid. A cell with a path length of 0.1 cm was used (Hellma, Kruibeke, Belgium). All spectra were corrected by subtracting the corresponding baseline. Concentration of PADI4 was the same used in the fluorescence experiments (1.5 μM, in protomer units).

(a) *Far-UV spectra*

Isothermal wavelength spectra at different pH values or GdmCl concentrations were acquired at a scan speed of 50 nm min^{-1} with a response time of 2 s, a band-width of 1 nm, and averaged over six scans. Both the chemical- and pH-denaturations were repeated at least three times with new samples. Buffer concentrations for the pH- and chemical-denaturation experiments were 50 mM, and the buffers (in the absence or presence of Ca^{2+}) were the same used in the fluorescence experiments (see above). Final glycerol concentration was 5% (v/v), and that of TCEP was 5 mM. In the pH-denaturations, the pH of each sample was measured after completion of titration with an ultra-thin Aldrich electrode in a Radiometer pH-meter. Variations from day to day of with the new prepared samples were less than 2%. The samples were prepared the day before and left overnight at 5 °C to allow for equilibration. Before starting the experiments, samples were left for 1 h at 25 °C.

(b) *Thermal-denaturations*

Experiments were performed at constant heating rates of 60 °C h^{-1} and a response time of 8 s. Thermal scans were collected by following the changes in ellipticity at 222 nm, typically from 25 to 70 °C. The rest of the experimental set-up was the same described in the steady-state experiments. No difference was observed between the scans aimed at testing a drift in the spectropolarimeter signal. Thermal denaturations were always irreversible, as shown by: (i) the comparison of spectra before and after the heating; and, (ii) the changes in the voltage of the instrument detector [38]. The apparent thermal denaturation midpoint, T_m, was estimated from a two-state equilibrium denaturation equation by taking into account the concentration-dependence of the unfolding equilibrium (see below).

(c) *Near-UV spectra*

Spectra of PADI4 either in the presence of Ca^{2+} (10 mM, final concentration) or in its absence (10 mM EDTA, final concentration) were acquired between 250 and 320 nm, in a 0.5-cm-pathlength cell at pH 7.5 (20 mM, Tris buffer, 5 mM TCEP, 150 mM NaCl and 5% glycerol) and

25 °C. The spectra were collected with a scan speed of 50 nm min^{-1} with a response time of 2 s, a band-width of 1 nm, and averaged over ten scans. The spectrum of the buffer solution was subtracted from that of the protein. Final protein concentration was 60 μM (in protomer units), under both conditions.

2.8. Differential scanning calorimetry (DSC)

The thermal stability of PADI4 was evaluated by DSC. The excess partial heat capacity of the protein in solution was measured as a function of temperature in an Auto-Cap-DSC (MicroCal, Malvern-Panalytical, Malvern, UK), using a constant heating rate of 60 °C h^{-1}. Experiments were done with PADI4 at 23.5 and 26.2 μM, in protomer units, in the absence and presence of Ca^{2+}, respectively, in 20 mM Tris buffer (pH 7.5), 5 mM TCEP, 150 mM NaCl and 5% glycerol. Buffer scans were performed until complete reproducibility was attained; the last measured buffer scan was subtracted from the protein scan. A model-free analysis provides an evaluation of the complexity of the observed unfolding pathway through the comparison of the calorimetric enthalpy (ΔH_{cal}, associated with the unfolding of the protein molecule) and the van't Hoff enthalpy (ΔH_{VH}, associated with the unfolding of the cooperative unit, defined as below, and the unfolding enthalpy corresponding to a two-state process). Whereas ΔH_{cal} is directly calculated as the area under the transition profile, ΔH_{VH} is calculated as follows:

$$\Delta H_{VH} = \frac{4RT_m^2 C_{P,max}}{\Delta H_{cal}} \tag{3}$$

where R is the ideal gas constant, T_m is the apparent unfolding temperature, and $C_{P,max}$ is the maximum value of the excess molar heat capacity. If $\Delta H_{VH} = \Delta H_{cal}$ (within experimental error), the cooperative unit coincides with the protein molecule (e.g., a protein domain) and the two-state model would be appropriate for the data analysis; if $\Delta H_{VH} < \Delta H_{cal}$, the cooperative unit is smaller than the protein molecule and the non-two-state model would be appropriate for the data analysis; and if $\Delta H_{VH} > \Delta H_{cal}$, the cooperative unit is larger than the protein molecule (i.e., the protein molecule self-associates into oligomers) and the dissociation-two-state model (e.g., oligomer unfolding coupled to dissociation into unfolded subunits) would be appropriate for the data analysis.

According to the two-state model (N ↔ U), the equilibrium unfolding process can be described by the following set of equations:

$$\begin{aligned}
K(T) &= \frac{F_U(T)}{F_N(T)} = e^{(-\Delta G(T)/RT)} \\
F_U(T) &= \frac{K(T)}{1+K(T)} \\
\Delta G(T) &= \Delta H(T_m)\left(1-\frac{T}{T_m}\right) + \Delta C_P\left(T - T_m - T\ln\frac{T}{T_m}\right) \\
\Delta H(T) &= F_U \Delta H(T) \\
\Delta C_P(T) &= \frac{\partial \Delta H(T)}{\partial T}
\end{aligned} \tag{4}$$

where K is the equilibrium unfolding constant; F_U and F_N are the fraction of unfolded and native protein molecules, respectively; ΔG is the unfolding Gibbs energy; ΔH is the unfolding enthalpy; ΔC_P is the unfolding heat capacity; $<\Delta H>$ is the excess average molar unfolding enthalpy; and $<\Delta C_P>$ is the excess average molar unfolding heat capacity (the observable provided by the calorimetric signal).

According to the dissociation-two-state model, particularized for a homodimeric protein (N_2 ↔ 2U), the equilibrium unfolding process can be described by the following set of equations:

$$\begin{aligned}
K(T) &= P_T\frac{(F_U(T))^2}{F_{N_2}(T)} = e^{(-2\Delta G(T)/RT)} \\
F_U(T) &= \frac{-1+\sqrt{1+8P_T/K(T)}}{4P_T/K(T)} \\
\Delta G(T) &= \Delta H(T_0)\left(1-\frac{T}{T_0}\right) + \Delta C_P\left(T - T_0 - T\ln\frac{T}{T_0}\right) \\
\Delta H(T) &= F_U \Delta H(T) \\
\Delta C_P(T) &= \frac{\partial \Delta H(T)}{\partial T}
\end{aligned} \tag{5}$$

where P_T is the total concentration of protein, and energy-related quantities have been defined per subunit. T_0 is the temperature at which the unfolding Gibbs energy is zero. In this case, $K(T)$ is the dissociation constant for the protein dimer. Contrary to what happens to the two-state model, in the case of an oligomeric protein, T_0 is different from T_m (temperature for maximal heat capacity) and $T_{1/2}$ (temperature for half-denaturation, $F_U = 0.5$).

Non-linear regression data analysis of the experimental data using Origin 7.0 (OriginLab, Northampton, MA, USA) allowed the estimation of the thermal unfolding parameters, from which the stability profile (ΔG as a function of T) can be constructed. In order to evaluate different models and establish the (statistically) most appropriate, parametric tests (e.g., F-test) and non-parametric tests (e.g., Akaike and Bayesian Information Criteria) were applied and compared.

2.9. Dynamic light scattering (DLS)

DLS measurements were performed in a Zetasizer Nano instrument (Malvern Instrument Ltd, Malvern, UK) equipped with a 10-mW helium-neon laser (λ = 632.8 nm) and a thermoelectric temperature controller. All the experiments were performed at a fixed angle (Θ = 173°) at 25 °C and the results were analysed with the Zetasizer software V7.12 (Malvern Instrument Ltd, Malvern, UK). Before each measurement, protein samples were centrifuged for 30 min at 14,000 g and filtered through a 0.2 μm cut-off Millex filter to remove big aggregates and dust. Once in the cuvette, samples were sonicated for 1 min to remove bubbles. Measurements on each sample were performed 20 times with 10 runs of 30 s each. The Z-average size was obtained by fitting the autocorrelation function with the cumulants method. The hydrodynamic radius, R_h, of the protein in solution was calculated by applying the Stokes-Einstein equation:

$$D = \frac{kT}{(6\,\pi\eta R_h)} \tag{6}$$

where k is the Boltzmann constant, T is the temperature and η is the solution viscosity. Experiments in the presence of 10 mM Ca^{2+} were carried out at 12 and 45 μM, in protomer units. Experiments in the absence of the cation (10 mM EDTA) were carried out at 8 and 25 μM, in protomer units. The buffer conditions were: 20 mM Tris (pH 7.5), 5 mM TCEP, 150 mM NaCl and 5% glycerol.

2.10. Fitting of pH-, chemical- and thermal-denaturations, followed by spectroscopic probes

In the fluorescence experiments, to allow for a better comparison among the different probes used (either intrinsic or ANS fluorescence), and since we can obtain information over all the spectrum, we calculated the average energy, <λ>, which is defined as [39]:

$$<\lambda> = \frac{\sum_1^n \left(\frac{1}{\lambda_i} I_i\right)}{\sum_1^n (I_i)} \tag{7}$$

The titration points for the pH-denaturation experiments were fitted

to the Henderson-Hasselbalch equation:

$$X = \left(X_a + X_b 10^{(pK_a - pH)}\right) / \left(1 + 10^{(pK_a - pH)}\right) \quad (8)$$

where X is the measured property (<λ>, the fluorescence intensity or the ellipticity at 222 nm) for a particular pH; X_a is the same property at low pH; X_b is the property at high pH; and pK_a is the titration midpoint of the pH-transition. When several transitions were observed, the different pK_a values were obtained by fitting each particular transition to Eq. (8), provided we had enough experimental data (at least >4 experimentally measured pH data points for the corresponding titration).

The change in the physical property, Y (the fluorescence intensity or the ellipticity at 222 or 230 nm), for the thermal denaturations, was fit to:

$$Y = \left(Y_N + Y_D e^{(-\Delta G/RT)}\right) / \left(1 + e^{(-\Delta G/RT)}\right) \quad (9)$$

where $Y_N = \alpha_N + \beta_N[T]$ and $Y_D = \alpha_D + \beta_D[T]$ are the baselines of the folded and unfolded states, respectively, for which a linear relationship with temperature is assumed; R is the gas constant; and T is the temperature in K.

Although the thermal denaturations, either followed by fluorescence (intrinsic, ANS or SYPRO Orange) or CD were irreversible, we obtained an apparent thermal denaturation midpoint, T_m, allowing us for a rough estimate of the stability of PADI4 at the different pH values, and for a comparison with the DSC data. The T_m can be obtained from the change in free energy, ΔG, given by [40–42]:

$$\Delta G(T) = \Delta H_m \left(1 - \frac{T}{T_m}\right) - \Delta C_p \left[(T_m - T) + Tln\left(\frac{T}{T_m}\right)\right] - RT \ln(2C_t) \quad (10)$$

where ΔH_m is the van't Hoff unfolding enthalpy; C_t is the total concentration of protein expressed in dimer equivalents; and ΔC_p is the heat capacity change of the folding reaction. The fact that both in the numerator and denominator of Eq. (9) appears the term $\Delta G(T)$ derived from Eq. (9) avoids to impose restrictions on the value of the ΔC_p used in the fitting. The term $-RT \ln(2C_t)$ comes from considering the dimeric nature of the protein (see Results) and it takes into account the concentration-dependence of the unfolding equilibria (both heat or chemical, see next paragraph) [40–42]; thus, we have assumed that the main species when thermal unfolding was carried out was a dimer.

For the GdmCl-denaturations (followed by intrinsic or ANS fluorescence and ellipticity at 222 nm) the same Eq. (9) was used, but in this case the value of the ΔG follows a linear relationship with respect to the denaturant concentration: $\Delta G = m$ ([GdmCl]$_{50\%}$ - [GdmCl]) - RTln(2C_t), where m-value is the slope of the sigmoidal transition; C_t is the total concentration of protein expressed in dimer equivalents; and [GdmCl]$_{50\%}$ is the concentration of GdmCl at the midpoint of the transition [43], and the spectroscopic properties of the native and unfolded species are given by: $Y_N = \alpha_N + \beta_N$[GdmCl] and $Y_D = \alpha_D + \beta_D$[GdmCl], respectively. Chemical denaturations were always irreversible, as indicated by refolding experiments.

Fittings to Eqs. (8)–(10) were carried out by using the general curve-fit option of KaleidaGraph (Abelbeck Software, PA, USA).

2.11. Molecular simulations

The structure of PADI4 was built from the PDB entry 3APN [31], and missing atoms in some loop regions were reconstructed by using the Modeller server [44]. Classical MD simulations of the protein in explicit solvent were performed by using the GROMACS software [45], with the AMBER ff99SB-ILDN force field [46] and the TIP3P water model [47]. The dimer was solvated in a box with a dodecahedron shape, maintaining a minimum distance of 1.5 nm from each edge, and 14 Na^+ counterions were added to obtain an overall neutral system charge. Simulations were carried out for 10 ns at room temperature (300 K, 27 °C), as well as at a higher value (450 K, 177 °C) to probe the early stages of the unfolding pathway through an accelerated sampling. Other details of the simulation conditions (including the modelling of electrostatic and van der Waals interactions, and the parameters used for the virtual thermostat and barostat), and of the simulation protocol (energy minimization, annealing, and equilibration) were as previously described [48,49].

Although MD runs can often be performed even at greater temperatures (T = 500 and beyond) [50], in this particular case this led to simulation crashes – which is not a rare occurrence, especially for very large protein systems. Thus, all-atom MD simulations at higher temperature could not be pursued further. Due to the excessive sampling required to probe more denatured protein states, the investigation was confined to the early steps of the unfolding, and we enhanced it by using a coarse-grained model implemented in the CABS-flex algorithm [51], available as a web server [52]. The starting structure of the dimer was the same used for MD simulations, with restraints assigned to residue pairs only when both possessed a well-defined secondary structure. In this case, we used a complete flexibility of the protein chain (assigning a null 'rigidity' parameter), and a dimensionless reduced temperature with a value (T = 2.0) twice larger than the default used to sample proteins in a crystal state to speed up the process [52].

3. Results

3.1. PADI4 expression in glioblastoma, pancreatic and colon cancer cells

It is known that PADI4 is expressed in a variety of adenocarcinomas, but absent in normal healthy tissues [53]. Moreover, it has been shown that plasma PADI4 levels in patients with malignancies decreased after tumour resection, suggesting that PADI4 circulating in the blood may be used for diagnostic of tumour tissues [54]. To address the prevalence of expression of PADI4 in cancer, protein levels were analysed and compared in a panel of tumour cell lines, that had never been tested before. We used pancreatic adenocarcinoma (PAAD) (RWP-1), colon adenocarcinoma (COAD) (HT-29) and glioblastoma (GBM) (GB-39) cell lines. This GBM cell line was obtained from a surgical wash from a patient that suffered multiforme GBM [34]. Western Blot analyses confirmed that the expression of PADI4 varied among the cancer cell lines. Out of the three lines examined, the PAAD one showed the least PADI4 expression (Fig. 1 A). Moreover, PADI4 expressions in COAD and GBM cell lines were of similar intensity, but with a different pattern (i.e. there were several bands in the GBM) consistent with the existence of alternatively spliced PADI4 transcripts [55].

Although most of PADI isoforms are cytoplasmatic, PADI4 has a nuclear localization signal (NLS) that allows it to enter the nucleus [2,54]. PADI4 first description in hematopoietic human cells shows a clear nuclear localization, however it can be also found in the cytoplasm depending on the cell line [56]. To investigate the subcellular localization of PADI4 in the above-mentioned cancer cell lines, we performed immunocytochemistry with PADI4 antibody and analysed it by fluorescence microscopy. PADI4 has an interesting nuclear localization pattern, and nuclei of the cells are characteristically stained with anti-PADI4 antibody at the nuclear edge. This distinctive signals of anti-PADI4 are usually confined to narrow diffuse DAPI-staining regions located along segmented forms of the nucleus (Fig. 1 B). Interestingly, PADI4 showed a clear nuclear localization only in HT-29 cells. PADI4 in GBM showed both a nuclear and cytoplasmatic expression; and in RWP-1, PADI4 expression was mostly cytoplasmatic and diffuse (Fig. 1 B). On the basis of these observations, together with the WB data, we hypothesize the presence of several forms of PADI4 with different subcellular localizations, depending on the cancer cell line.

The tumour suppressor p53 plays a pivotal role in regulating the cell cycle progression and apoptosis in response to various genotoxic and nongenotoxic stresses [56]. The ability of p53 to function as a sequence-specific transcription factor is critical for its tumour suppressor function [57]. It has been shown that PADI4 interacts with p53 and is

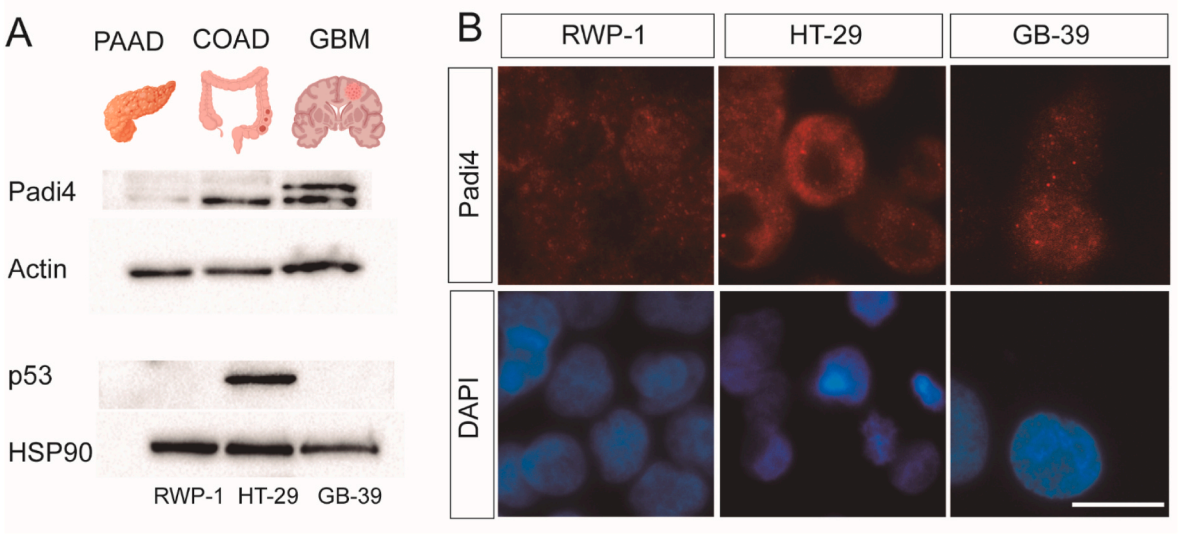

Fig. 1. PADI4 expression in cancer cells lines. (A) Western blot analysis of RWP-1, HT-29 and GB-39 cell lines for PADI4 and p53. (B) Immunocytochemistry of PADI4 (red) and DAPI (blue) in cancer cell lines. Scale bar: 20 μm. Experiments were repeated three times. (For interpretation of the references to color in this figure legend, the reader is referred to the Web version of this article.)

recruited by the p21 promoter to regulate histone arginine-methylation and citrullination to regulate gene expression [24]. Therefore, we investigated the relationship between PADI4 and p53 in the three cancer cell lines described above. We observed a large expression of p53 in HT-29, but not in the other cell lines (Fig. 1 B). Thus, based on two different lines of evidence: (i) HT-29 was the sole cell line with a clear nuclear localization of PADI4; and (ii) the distinct enzyme expression observed in the WB data, we suggest that PADI4 could have a major role in tumorigenesis by up-regulating p53 expression in certain types of cancer cell types.

3.2. *PADI4 acquired a native structure in a narrow pH range either in the absence or in the presence of Ca^{2+}*

To measure the conformational stability of PADI4, we firstly needed to determine in which pH range it had a native structure. To that end, we used several spectroscopic probes, namely intrinsic fluorescence, ANS fluorescence, and far- and near-UV CD. The use of this whole set of techniques gave us complementary information on different structural features of the polypeptide chain. We used intrinsic fluorescence to monitor the changes in the tertiary structure of PADI4, around its 13 tyrosines and 10 tryptophans. We used ANS fluorescence to follow the water accessibility of solvent-exposed hydrophobic patches and to detect the presence of partially folded species [58]. And finally, we carried out far-UV CD experiments to monitor changes in protein secondary structure, and near-UV CD to follow the changes in the asymmetry of the environment around aromatic residues at a determined pH.

3.3. *Fluorescence*

(1) *Steady-state intrinsic fluorescence and thermal denaturations*

The fluorescence emission spectrum of PADI4 showed a maximum around 338 nm at physiological pH in the absence of Ca^{2+} (Fig. S1 A). These results indicate that PADI4 fluorescence was dominated by the emission of the 10 tryptophan residues, some of which appeared, from the value of the maximum wavelength, to be partially solvent-exposed, as also shown in the X-ray structure deposited in the Protein Data Bank (PDB) as the entry 3APN [31]. A red-shift of the signal maximum in the presence of Ca^{2+} (towards 342 nm) was observed, as well as a decrease in the intensity (Fig. S1). The same changes were also observed by excitation at 295 nm, indicating that some tryptophan residues were located in the polypeptide regions involved in the binding of Ca^{2+}. This result suggests that the environment of at least some of the tryptophans and/or tyrosines were altered in the presence of Ca^{2+}, resulting in a more solvent-exposed species.

The value of $<\lambda>$ (measured either by excitation at 280 or 295 nm) in the presence of EDTA (10 mM) showed two transitions (Fig. 2 A): one appeared to end around pH 6.5, but we could not find its pK_a value due to the absence of an acidic baseline; and another one started at pH 8.0, which had a pK_a value larger than 10, but we could not assess its exact value as we could not determine a basic baseline. The same two transitions were observed by following the changes in intensity (Fig. 2 A), and a dumb-bell shape was detected on the whole pH range for the intensity variations. We followed the changes in intensity at pH 7.5 (in the middle of the interval where the protein seemed to possess a tertiary native structure: pH 6.5–8.0) by thermal denaturations; an irreversible, sigmoidal thermal transition was observed with a T_m of 57.7 ± 0.3 °C, whose value was obtained from Eq. (10) (Fig. S1 B). No sigmoidal transitions were observed outside that pH interval (data not shown).

On the other hand, the fluorescence spectra in the presence of Ca^{2+} were noisier than those in the presence of EDTA (Fig. S1 A), and therefore the pH data from the titrations were more scattered. The $<\lambda>$ (either by excitation at 280 or 295 nm) in the presence of Ca^{2+} showed two transitions as well (Fig. 2 B), starting and finishing roughly at the same pH values as the transitions found in the presence of EDTA. Similarly, the same two transitions at acidic and basic pH values were observed by following the changes in intensity (Fig. 2 B). We also performed fluorescence thermal denaturations in that pH range (6.5–8.0), as well as outside that interval. No sigmoidal transitions were observed by fluorescence (data not shown), and the irreversible transitions observed in that pH interval were less co-operative (that is, they were flatter than those observed in the presence of 10 mM of EDTA). Attempts to fit those curves to Eq. (10) yielded a T_m of 73 ± 5 °C (Fig. S1 B).

Therefore, it seems that, regardless of the absence or the presence of Ca^{2+}, the same titrating residues are determining the features of the tertiary structure around tryptophan and tyrosine residues at both extremes of pH, but the presence of Ca^{2+} changed the environment around at least some of the indole or phenol moieties.

(2) *ANS-binding*

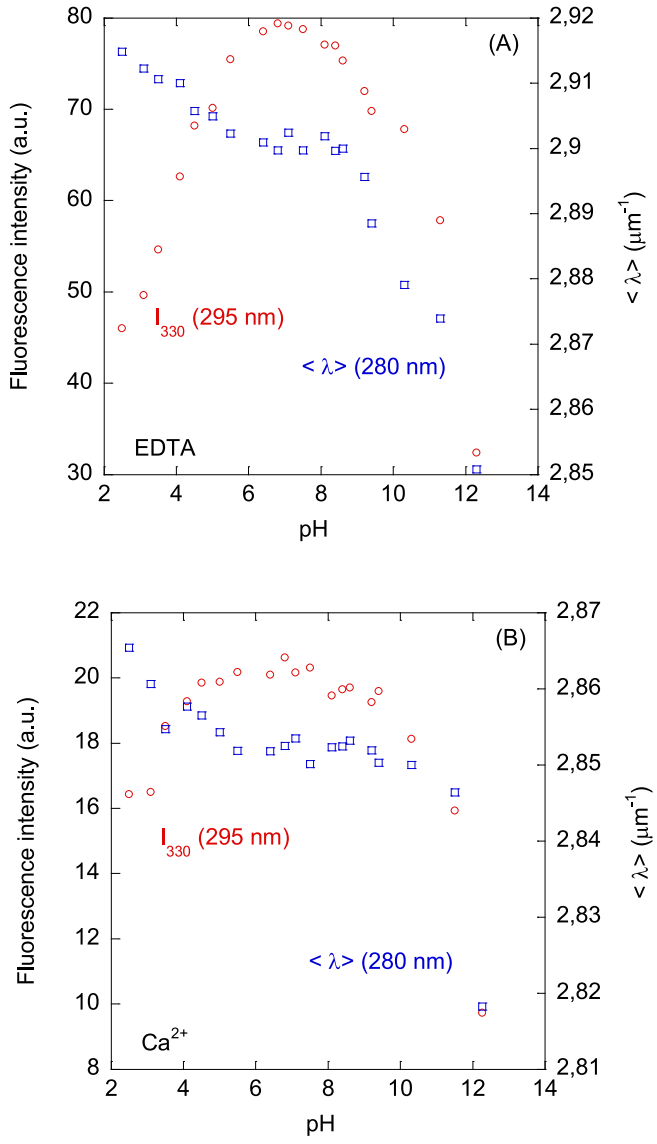

Fig. 2. pH-induced structural changes of PADI4 followed by intrinsic fluorescence: Conformational changes of PADI4 monitored by the intrinsic fluorescence at 330 nm, after excitation at 295 nm (blank, red circles) and by <λ> (average energy), after excitation at 280 nm (blank, blue squares) in the presence of EDTA (A), and in the presence of Ca^{2+} (B). (For interpretation of the references to color in this figure legend, the reader is referred to the Web version of this article.)

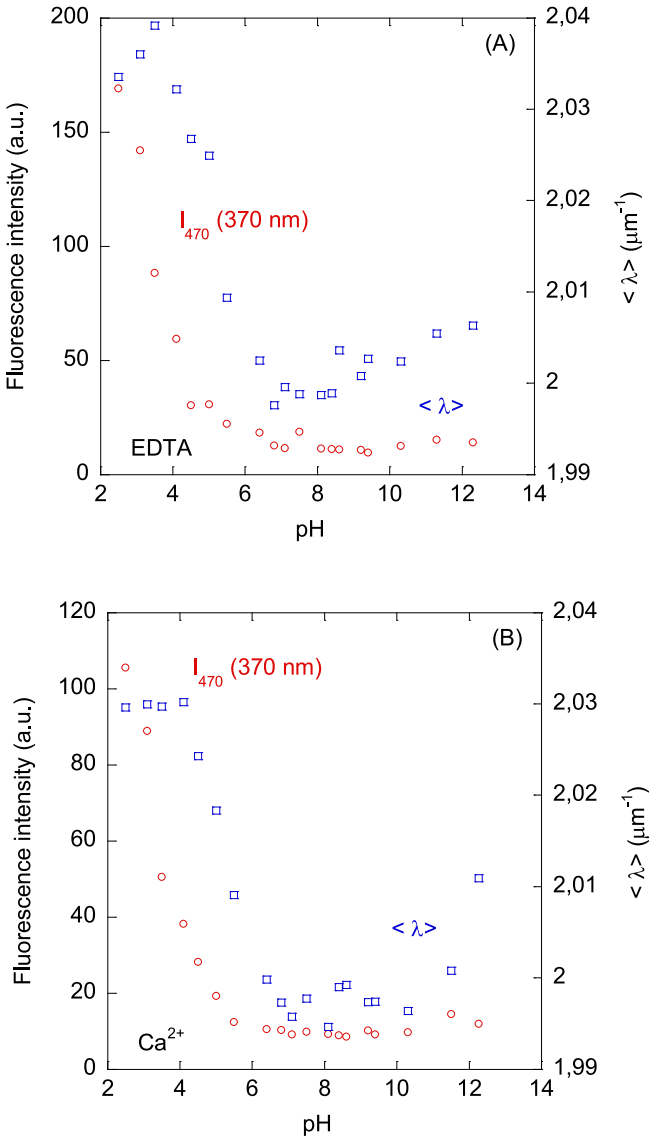

Fig. 3. pH-induced structural changes of PADI4 followed by ANS fluorescence: Conformational changes of PADI4 monitored by ANS fluorescence at 470 nm, after excitation at 370 nm (blank, red circles) and by <λ> (blank, blue squares) in the presence of EDTA (A), and in the presence of Ca^{2+} (B). (For interpretation of the references to color in this figure legend, the reader is referred to the Web version of this article.)

We also observed two transitions in the pH-titrations (either in the presence or absence of Ca^{2+}) followed by ANS (Fig. 3 A). In the presence of EDTA, conversely to what we had observed by following the intrinsic fluorescence of the protein, the pK_a of the acidic transition, obtained following <λ>, was 5.3 ± 0.5; in contrast, by following the intensity, we could not determine the pK_a because we did not have an acidic baseline. This acidic transition was completely finished at pH ~6.5. The basic transition, which started at pH ~8.0, was clearly observed by following <λ>, but such transition could not be monitored by following the intensity at 470 nm.

On the other hand, in the presence of Ca^{2+}, the pK_a of the acidic transition followed by <λ> was 5.9 ± 0.6 (Fig. 3 B), similar to that observed in the presence of EDTA. We could not determine the pK_a of this acidic transition from the changes in the fluorescence intensity, due to the lack of an acidic baseline. This acidic transition ended at pH ~6.5. At basic pH values, as it happened in the presence of EDTA, the transition was more clearly observed by monitoring <λ> rather than the fluorescence intensity; this transition started at pH ~8.0, but we could not determine its pK_a due to the absence of baseline.

Thermal denaturations following the ANS fluorescence, at different pH values in the presence of EDTA, showed only a single sigmoidal transition (Fig S2 A). The apparent T_m value at pH 7.5 was 56.8 ± 0.3 °C, identical to that measured by intrinsic fluorescence at the same pH. On the other hand, in the presence of Ca^{2+}, we also observed only a sigmoidal transition for pH values between 6.5 and 8.0 (Fig. S2 B); at pH 7.5, we obtained a T_m value of 52 ± 4 °C.

Therefore, we can conclude that the variation monitored by ANS in the burial of solvent-exposed hydrophobic surface occurred concomitantly to that of the acquisition of tertiary structure, monitored by the intrinsic fluorescence of tryptophans and tyrosines, during protein folding.

(3) *DSF*

We also carried out measurements in the presence of the fluorescent dye SYPRO Orange as protein unfolding reporter. Our results (Fig. S3 A) indicate that the fluorescence of this extrinsic probe was higher in the presence of EDTA than when Ca^{2+} was present, suggesting solvent-exposure of hydrophobic regions in the Ca^{2+}-free protein. Thermal denaturation experiments further suggest that the Ca^{2+}-free protein exhibited an apparent single transition centred at 57 °C (similar to the values observed by monitoring the intrinsic and ANS fluorescence, see above), whereas the Ca^{2+}-bound protein exhibited two transitions centred at 59 and 71 °C, respectively (Fig. S3 B). The former value was similar to that obtained from ANS fluorescence in the presence of Ca^{2+}, and the latter was similar to that obtained by intrinsic fluorescence (see above). An apparent unfolding enthalpy of 45 kcal mol^{-1} for the Ca^{2+}-free protein could be estimated from the derivative of the curve expressing the unfolded fraction at such T_m (Eq. (9)). This value is relatively small for a 74 kDa protein protomer suggesting: (i) a non-complete unfolding of the protein upon heating in the presence of this probe; or alternatively, (ii) a considerable level of flexibility, in agreement with the exposure of hydrophobic surface detected in the steady-state spectra (Fig. S3 A) (see Discussion). It could be argued that such small value of the apparent unfolding enthalpy might be due to a disordered nature of the protein; however, the fact that intrinsic fluorescence and far-UV CD spectra (see below) were those of a typical folded protein with buried tryptophan residues suggests that such small enthalpy value was due to any of the reasons indicated above.

Far-UV CD: The CD spectrum of PADI4 in the absence of Ca^{2+} at pH 7.5 showed minima at 210 and 222 nm (Fig. S4 A). These results indicate that the protein had mainly a helical fold, as well as a fraction of β-sheet structure, in agreement with its X-ray structure (PDB entry 3APN [31]). We estimated the percentage of helical structure by assuming that, at 222 nm, a 100% amount of fully formed helical structure determines a molar ellipticity, [Θ], of −39500 deg cm^2 $dmol^{-1}$ [59]. The $[\Theta]^{222}$ of PADI4 at pH 7.5 was −2668 deg cm^2 $dmol^{-1}$, yielding an estimated value of 7% of helical structure. The value obtained from the X-ray structure (PDB number: 3APN), where 112 residues out of 651 (per monomer) are in an α-helix conformation, was 17%. Besides uncertainties in the determination of secondary structure by using CD data, the main difference in the amount of helical structure calculated from the X-ray and from experimental far-UV CD data could be attributed to the presence of aromatic residues, which also absorb at 222 nm in the far-UV CD spectrum [60–63]. We could not acquire a good far-UV CD spectrum of PADI4 in the presence of Ca^{2+}, since its presence precluded having any meaningful information for wavelengths below 215 nm.

In the following, we shall not try to over-interpret the CD results, and we shall report on those changes which are clearly observable and are also supported, to some extent, by the results from fluorescence (either in the intrinsic or ANS experiments). In the pH-titrations followed by the raw ellipticity at 222 nm (Θ^{222}), either in the absence or presence of Ca^{2+}, we also observed two transitions (Fig. 4). We had to observe the changes in ellipticity in the presence of Ca^{2+} at 230 nm, due to the poorer signal-to-noise ratio at 222 nm (because of the presence of the salt). The first acidic transition resulted in an increase of the helicity (in absolute value) as the pH was raised, under either condition. These findings mean that the protein has lost its secondary structure, as monitored by far-UV CD, at acidic conditions. In the presence of EDTA, the first acidic transition had a pK_a of 5.1 ± 0.4 (Fig. 4 A); whereas in the presence of Ca^{2+}, the transition was at 5.6 ± 0.3 (Fig. 4 B). The two values are similar, within the fitting error to the Henderson-Hasselbalch equation (Eq. (8)), and comparable to those obtained by ANS fluorescence (see above). Under both conditions, we also observed that at basic pH values there was a decrease in the ellipticity at 222 nm (in absolute value) as the pH was raised (Fig. 4), but we could not determine the pK_a value, as we did not have a basic baseline. Therefore, to sum up, we can conclude that acquisition of secondary structure, as monitored by far-UV CD, occurred concomitantly to that of tertiary structure (intrinsic fluorescence) and the burial of solvent-exposed hydrophobic surface (ANS

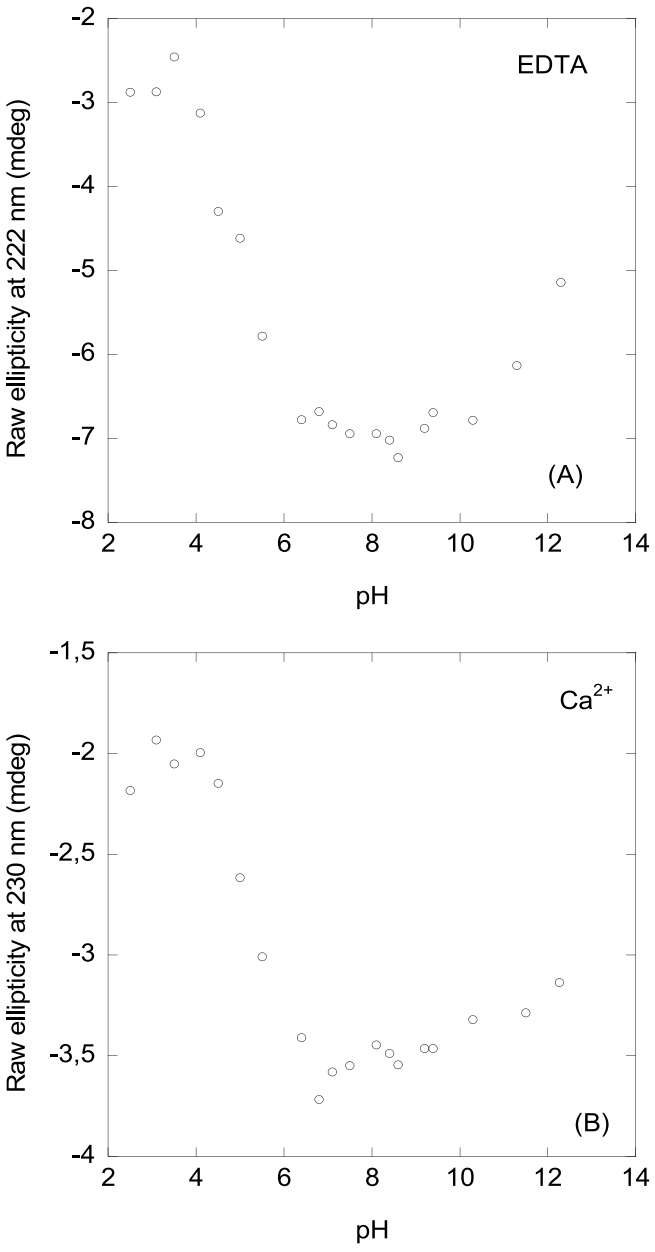

Fig. 4. pH-induced structural changes of PADI4 followed by far-UV CD: Conformational changes of PADI4 monitored by the raw ellipticity at 222 nm in the presence of EDTA (A), and in the presence of Ca^{2+} (B).

fluorescence) under both solution conditions (in the absence and presence of Ca^{2+}) and moving towards physiological conditions starting from either acidic or pH values. Thus, the acquisition of native structure only occurred in a narrow pH interval (Figs. 2–4).

Thermal denaturations in the pH interval where PADI4 acquired a native structure were characterized, in the presence of Ca^{2+}, by a poor signal-to-noise ratio, thus precluding any reliable determination of T_m. On the other hand, in the presence of EDTA at pH 7.5 (Fig. S4 B), the irreversible, single sigmoidal denaturation curve yielded a T_m value of 52.9 ± 0.7 °C. This value was smaller than those obtained by intrinsic, ANS and SYPRO Orange fluorescence (see above); however, it was similar to that obtained for wild-type PADI4 under similar conditions reported by other laboratories [31]. These findings might suggest that secondary structure, as monitored by far-UV CD, melted before the tertiary one, in contrast of what one could expect (i.e., tertiary structure melting before the secondary one). This apparent discrepancy is due to

the strong irreversibility of the thermal denaturation, and it has also been observed in thermal denaturations of other large proteins [64–66]. It could be argued that the irreversibility can either be inherent to the unfolding process (i.e., concomitant with the unfolding) or occur at high temperatures much later than the unfolding process. This can be tested by performing an unfolding experiment up to the apparent T_m, and then reheating. If the reheating recovers most of the unfolding trace, the unfolding can be considered reversible, even if maintaining the protein at higher temperatures would result in an irreversible process. Furthermore, the irreversibility can be assessed in the far UV CD experiments by monitoring the voltage as the thermal unfolding progresses [38]. If the voltage follows a linear-temperature dependence, it indicates that the unfolding is reversible; on the other hand, if it shows a sigmoidal-like behaviour (as that observed for the ellipticity) then the process is irreversible indicating aggregation. We used both procedures for PADI4: the first one by following intrinsic fluorescence of the protein and the second one by using far-UV CD. In the case of fluorescence, stopping the thermal scan at the apparent midpoint did not result in recovering neither the original fluorescence intensity of the spectrum at 25 °C (Fig. S1 A) nor a sigmoidal-like scan (Fig. S1 B) under both solution conditions. In the case of far-UV CD, we observed a sigmoidal-like behaviour in the voltage of the instrument with an apparent midpoint at 53 °C (close to the value observed by following the ellipticity at 222 nm). Then, we suggest that unfolding of PADI4 is associated with aggregation (that is, a temperature higher than the apparent T_m is not necessary to achieve self-association of the unfolded protein).

Near-UV CD: We only carried out near-UV experiments at pH 7.5 in the absence and in the presence of Ca^{2+}. PADI4 has a large number of aromatic residues (10 tryptophans, 13 tyrosines, 33 phenylalanines and 15 histidines in its sequence) and thus, the near-UV CD spectrum under both conditions had a large intensity [60–63]. The near-UV spectrum of PADI4 showed a broad maximum peak around 265 nm (Fig. S5), and a minimum at 297 nm. The normalized ellipticity was larger (in absolute value) for the spectrum in the presence of Ca^{2+} than in the presence of EDTA, thus confirming the previous findings obtained by intrinsic fluorescence, that the local environment around some of the tryptophan residues changed in the presence of the cation (Fig. S1 A).

To sum up, based on the findings obtained with the different spectroscopic probes used, we can conclude that the secondary and tertiary structures of PADI4 are lost concomitantly when moving to the two extremes values of pH. Thus, the pH range where PADI4 acquired a native structure was very narrow, encompassing an interval from 6.5 to 8.0.

3.4. PADI4 was a dimer in aqueous solution at physiological pH both in the absence and the presence of Ca^{2+}

DLS measurements of PADI4, in the absence and presence of Ca^{2+}, were performed at different concentrations ranging from 8 to 45 μM (in protomer units). The samples showed a small amount of high molecular weight aggregates: lower than 1% in the samples in the presence of the cation, and lower than 5% in the presence of EDTA. In the range of PADI4 concentrations assayed, its hydrodynamic radius (R_h) did not change in presence of Ca^{2+} when compared to that in the presence of EDTA (Fig. 5). The average R_h values of PADI4 under the different assayed conditions were: (i) in the presence of EDTA: $R_h = 5.4 \pm 1.1$ nm (8 μM) and 5.1 ± 0.6 nm (25 μM); and, (ii) in the presence of Ca^{2+}: $R_h = 5.1 \pm 1.1$ nm (12 μM) and 5.6 ± 0.6 nm (45 μM). The estimated molecular weight by using the Stokes-Einstein equation (Eq. (6)) for a protein with $R_h = 5.1$ nm is approximately 150 kDa, which indicates the presence of a dimer of PADI4 in solution under both conditions (the molecular weight of the monomer is 74.0 kDa). These results agree with previous findings obtained under slightly different conditions [67], and confirm that in solution PADI4 is a dimer as in the crystal structure [30, 31].

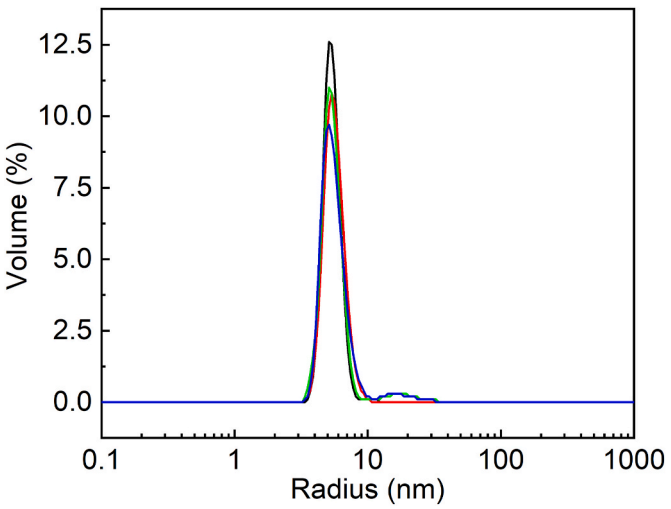

Fig. 5. DLS measurements of PADI4: The DLS volume distribution profiles of PADI4 in presence and absence of Ca^{2+}: (black line) at 12 μM in the presence of Ca^{2+}; (red line) at 45 μM in the presence of Ca^{2+}; (green line) at 8 μM in the presence of EDTA; and (blue line) at 25 μM in the presence of EDTA. (For interpretation of the references to color in this figure legend, the reader is referred to the Web version of this article.)

3.5. Conformational stability of PADI4

We proceeded to measure the conformational stability of PADI4 by using heat (*via* DSC), and chemical denaturation followed by intrinsic and ANS fluorescence and far-UV CD at pH 7.5. Our previous results indicate that thermal denaturations of PADI4 were irreversible and that stability of PADI4 at such pH in the presence of EDTA was not very high (see above). Even though the thermal denaturations seemed to be irreversible, the irreversibility may stem from additional processes different from the unfolding process (e.g., aggregation of the unfolded conformation). In that case, although the application of equilibrium models is problematic, still those models provide useful estimates of the thermal stability parameters. Furthermore, we aimed to obtain an estimate of the stability of PADI4 by using far-UV and fluorescence, either in the absence or the presence of Ca^{2+}, by using a chemical agent as denaturant.

3.5.1. A calorimetric point of view

The DSC experiments of PADI4 in the absence and presence of Ca^{2+} are shown in Fig. 6. The presence of Ca^{2+} induces a more complex unfolding behaviour; it may be possible that, because the unfolding shifts to higher temperatures, the irreversibility of the process might be more pronounced at those higher temperatures, hindering a reasonable analysis. Still, a considerable stabilization effect induced by Ca^{2+} binding could be observed: an apparent T_m value of 53.2 °C without Ca^{2+}; and two apparent T_m values of 59.6 and 72.6 °C were observed when the cation was present. The single T_m observed in the absence of Ca^{2+} and the highest T_m observed in the presence of Ca^{2+} are similar to those observed by fluorescence thermal denaturations (see above).

The model-free analysis provided apparent values for the thermal stability parameters: ΔH_{cal} value of 86 kcal mol^{-1}, and $C_{P,max}$ value of 11.1 kcal K^{-1}·mol^{-1}, from which a ΔH_{VH} value of 109 kcal mol^{-1} could be estimated. From those figures, an enthalpy ratio of 1.27 could be calculated, which differs from unity beyond the experimental error. Importantly, the unfolding trace is slightly asymmetric, with a negative skew, as typically observed in the unfolding of homooligomeric proteins. Therefore, the most appropriate model for analysing the unfolding process of PADI4 is that of a protein dimer unfolding and dissociating simultaneously into unfolded subunits.

Fig. 6 shows the calorimetric thermal unfolding of PADI4 in the

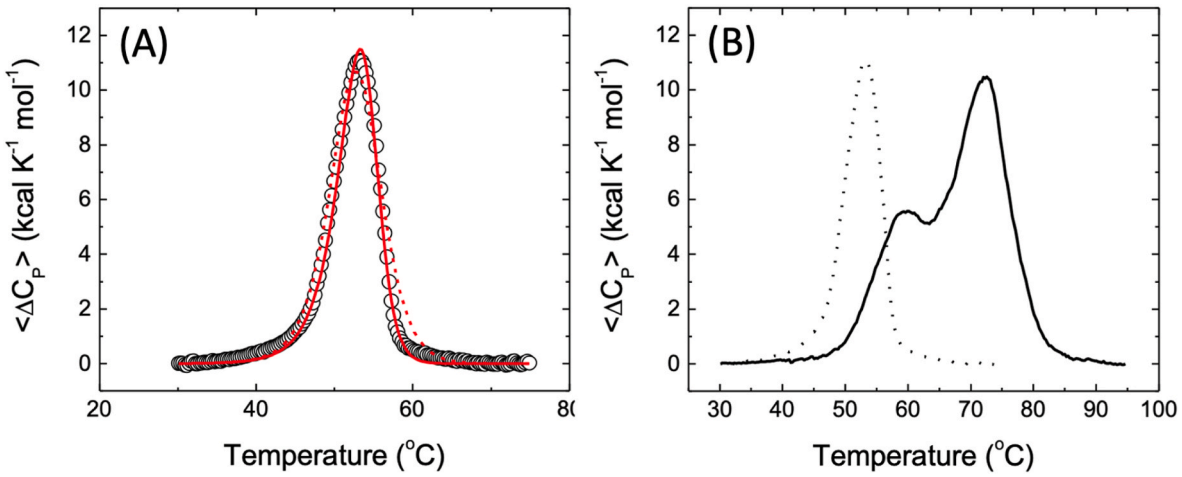

Fig. 6. DSC experiments: (A) Thermal denaturation of PADI4 in the absence of Ca^{2+}. A single apparent unfolding transition is observed. The experimental data (empty circles) were analysed according to a two-state model (dashed red line) and a two-state-unfolding-dissociation model (continuous red line). (B) Thermal denaturation of PADI4 in the presence of Ca^{2+} (continuous black line). The unfolding, in the absence of Ca^{2+} (dotted line), is shown for comparison. (For interpretation of the references to color in this figure legend, the reader is referred to the Web version of this article.)

absence of Ca^{2+} analysed with the two-state model ($T_m = 52.2 \pm 0.2$ °C, $\Delta H(T_m) = 94 \pm 2$ kcal mol^{-1}) and with the unfolding-dissociation model ($T_0 = 64.0 \pm 0.3$ °C, $\Delta H(T_m) = 117 \pm 2$ kcal mol^{-1}). It is important to note that the T_0 obtained by using the dissociation model corresponds to the temperature at which the Gibbs energy of unfolding becomes zero, which, for a dimeric protein, it is much higher than the T_m, the temperature for maximal unfolding heat capacity, which corresponds to the temperature estimated by spectroscopic measurements (see above); in fact, the apparent T_m values observed using the different techniques (spectroscopy and calorimetry) are very similar. Therefore, this finding indicates that the apparent thermal denaturation midpoint determined by spectroscopy was probably strongly affected by protein self-association. The fitting was visually much better for the unfolding dissociation model, but also statistically better considering the residual-sum-of-squares (RSS), with values of $4.9{\cdot}10^7$ and $1.1{\cdot}10^7$, for the two-state model and the unfolding-dissociation model, respectively. The thermal stability parameters were used for extrapolating the unfolding Gibbs energy and the equilibrium unfolding constant from 64 to 25 °C, and a dissociation constant for the PADI4 dimer of 0.9 ± 0.4 μM was estimated at 25 °C, a value in agreement with the one previously reported from analytical ultracentrifugation (AUC) experiments [67].

3.5.2. *A chemical-denaturation point of view*

Chemical refolding experiments using GdmCl as denaturant, indicated that unfolding of PADI4 was not reversible. Therefore, we could not obtain the free energy (ΔG) of the unfolding reaction, and we will not be able to discuss quantitatively the unfolding mechanism of PADI4.

Firstly, we tried, in the presence of EDTA, to determine whether urea or GdmCl was better suited to follow the chemical unfolding of PADI4. Experiments using urea as denaturant agent showed that, when using $\langle\lambda\rangle$ (or the intensity) of the intrinsic fluorescence as the physical quantity to follow the denaturation, no transition was observed, but rather an un-cooperative, flat transition without any native or unfolded baselines of the curve (Fig. S6). On the other hand, the ellipticity at 222 nm in the urea-denaturations showed two transitions: one occurring at low urea concentration, and the other occurring with an $[urea]_{1/2}$ of 4.1 ± 0.3 M (Fig. S6). These findings suggest that the chemical unfolding of PADI4, due to its large size, is complex. Due to the lack of a clear transition when PADI4 unfolding was monitored using urea by fluorescence, we decided to use GdmCl as a chaotropic agent.

Chemical denaturations by using GdmCl as denaturant showed, as well, a complex behaviour when the ellipticity at 222 nm was monitored, with at least three transitions (Fig. 7 A); one of them, as it happened for experiments with urea, occurring at low denaturant concentrations. Conversely, the GdmCl-denaturations followed by fluorescence (either $\langle\lambda\rangle$ or the intensity) showed a single, very broad transition, with $[GdmCl]_{1/2} = 0.9 \pm 0.5$ M and $m = 0.9 \pm 0.3$ kcal mol^{-1} M^{-1} (at 280 nm), suggesting that PADI4 was a protein with low stability. We also followed the GdmCl-denaturations by using ANS as a probe (Fig. 7 B), yielding $[GdmCl]_{1/2} = 1.52 \pm 0.09$ M and $m = 2.1 \pm 0.4$ kcal mol^{-1} M^{-1}. These values are different from those obtained by following the intrinsic fluorescence, indicating that the denaturation of PADI4 in the presence of EDTA was complex. Furthermore, as PADI4 is a dimer, we hypothesized that some of the transitions observed in the far-UV CD spectra could be due to dimer dissociation, and then, this reaction could be better observed at higher protein concentrations used during the experiments. Therefore, we carried out a chemical denaturation experiment at a protein concentration of 10.5 μM, in protomer units (Fig. S7), but even at this value we were not able to resolve the different transitions observed at low protein concentration. These results suggest that the dissociation constant of the PADI4 dimer was smaller than the lowest protein concentration (in protomer units) used in our chemical denaturation experiments; in fact, AUC experiments have shown that such constant has a value of 0.45 μM at 20 °C [67], in agreement with the value estimated from our DSC experiments (see above). The thermal stability of PADI4 seems to be much lower from the spectroscopic assays (ΔG value of 0.8 kcal mol^{-1} from tryptophan intrinsic fluorescence thermal denaturations, and a value of 3.2 kcal mol^{-1} from ANS extrinsic fluorescence thermal denaturations) compared to the value estimated from DSC experiments (ΔG value of 4.1 kcal mol^{-1}) and that estimated from AUC experiments (ΔG value of 4.3 kcal mol^{-1}). This may be due to the local nature of the protein features determining the spectroscopic signal, compared to the global nature of the DSC and AUC observable signals.

On the other hand, chemical denaturation experiments of PADI4 carried out in the presence of Ca^{2+} did not yield sigmoidal transitions (i.e., we observed a non-cooperative behaviour) when followed by fluorescence or ellipticity at 222 nm (Fig. 8 A), suggesting that the unfolding of the protein under these conditions was less co-operative than in the presence of EDTA. Furthermore, by using ANS as a probe, we obtained $[GdmCl]_{1/2} = 2.02 \pm 0.08$ M and $m = 1.9 \pm 0.4$ kcal mol^{-1} M^{-1} (Fig. 8 B), which yields an apparent ΔG value larger than that obtained in the presence of EDTA, and in agreement with the DSC data (Fig. 6), where we observed a stabilization of the protein. Therefore, the presence of Ca^{2+} induced changes in the tertiary environment around some aromatic residues (see above), as well as variations in the solvent-exposed

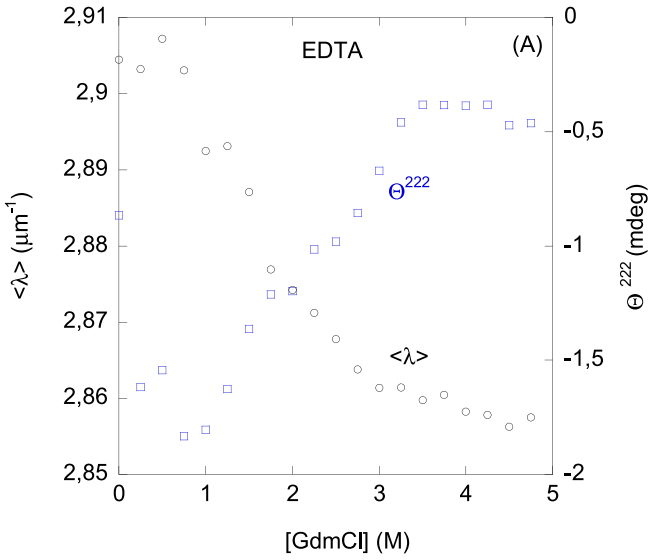

Fig. 7. Chemical denaturations of PADI4 in the presence of EDTA followed by spectroscopic techniques. (A) Conformational changes of PADI monitored by <λ>, after excitation at 280 (filled, black circles), and by the ellipticity at 222 nm (blue, blank squares). (B) Conformational changes of PADI4 monitored by the changes in the intensity at 470 nm of the ANS probe (after excitation at 370 nm). The line through the ANS fluorescence data is the fitting to a two-state model according to Eq. (9). (For interpretation of the references to color in this figure legend, the reader is referred to the Web version of this article.)

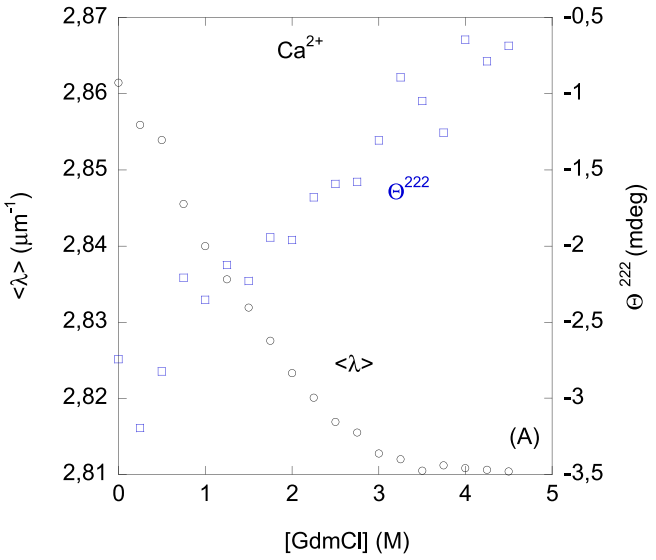

Fig. 8. Chemical denaturations of PADI4 in the presence of Ca^{2+} followed by spectroscopic techniques. (A) Conformational changes of PADI monitored by <λ>, after excitation at 280 (filled, black circles), and by the ellipticity at 222 nm (blue, blank squares). (B) Conformational changes of PADI4 monitored by the changes in the intensity at 470 nm of the ANS probe (after excitation at 370 nm). The line through the ANS fluorescence data is the fitting to a two-state model according to Eq. (9). (For interpretation of the references to color in this figure legend, the reader is referred to the Web version of this article.)

surface. These results indicate that the solvent-exposure of hydrophobic regions of PADI4 was different from that observed in the presence of EDTA. These findings are confirmed by the X-ray structures of PADI4 in the absence (PDB number: 1APN) and in the presence of Ca^{2+} (PDB number: 1WD9). Furthermore, since by AUC experiments no quaternary structure stabilization was observed in the presence of Ca^{2+} [67], we suggest that the changes in stabilization observed by chemical denaturation (Fig. 8) and DSC (Fig. 6) were due to stabilization of the secondary and/or tertiary structure within the monomer (see Discussion).

3.6. Flexibility of the protein structure in molecular simulations

Molecular simulations were used to elucidate the flexibility of PADI4, which was observed to have peculiar characteristics on the basis of our experimental findings (see above). A low rigidity of the protein structure could play a mechanistic role in determining its low stability and, from a functional point of view, could favor the interaction with various molecular partners. To investigate this aspect, we employed MD simulation, which is one of the most direct techniques to probe the dynamics of a protein [50]. The PADI4 dimer was observed on the time scale of 10 ns, which was adequate to equilibrate the deviations of the atomic positions with respect to the starting structure (Fig. S8, black line). The results reported in Fig. 9 show the root mean square fluctuations (RMSF) of the atomic positions of the C^{α} atoms as a function of the residue number. The data shown are averaged on the two monomers; therefore, they tend to evidence non-random, coordinated motions of relatively long (>10 residues) portions of PADI4 sequence. At room temperature (Fig. 9 A, black line), the stiffer regions of PADI4 have fluctuations of ~0.1 nm, whereas the most flexible regions can reach values up to ~0.3 nm. It is immediate noticeable that the fluctuations were almost evenly distributed on the whole sequence, despite the presence of extended protein regions with different secondary (α/β) and

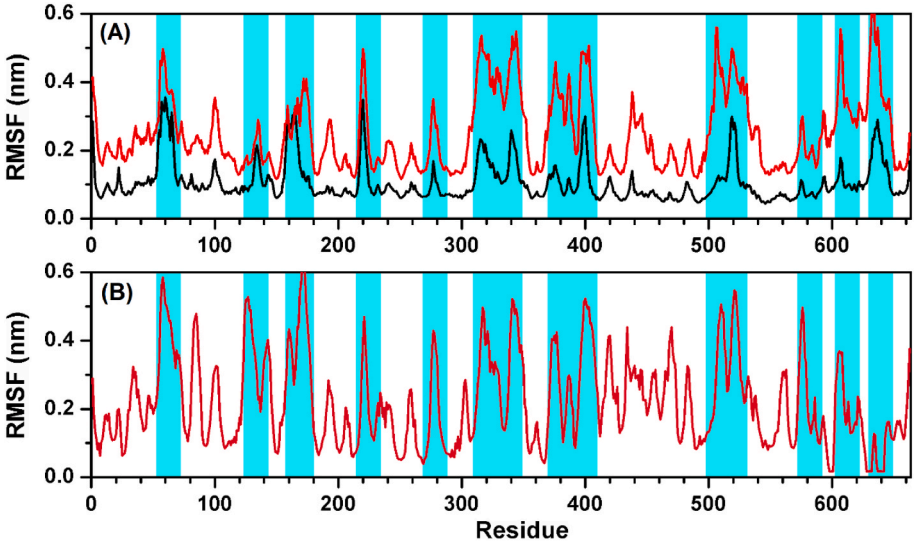

Fig. 9. Simulated average RMSF of the backbone atomic position of PADI4. (A) MD simulations at (black line) 300 K and (red line) 450 K. (B) Coarse-grained simulation using the CABS-flex model [51], with dimensionless reduced T = 2.0. Regions ≥20 residues highlighted in cyan have RMSF >0.4 and/or 0.5 nm in MD and CAB-flex modeling, respectively. Values are calculated in all cases by simulating the dimeric structure and averaging the fluctuations obtained for the two monomers. (For interpretation of the references to color in this figure legend, the reader is referred to the Web version of this article.)

tertiary structure (three distinct subdomains) [30]. High-temperature MD simulation was also used to investigate the early steps of the protein unfolding; to speed up the process, a simulation value of 450 K was used, as it is common practice [68,69]. The results (Fig. 9 A, red line) indicated that the RMSF of the atomic positions were about twice larger compared to those at room temperature, for both the most rigid and flexible protein regions. In particular, the highest fluctuation values were found in correspondence with the same regions showing relatively high motions also at room temperature. This observation confirms that the flexibility of PADI4 remained evenly distributed on the whole structure when the temperature was increased.

Besides the local unfolding of the protein structure in a few selected regions, the simulation temperature of 450 K was insufficient to observe the melting of the whole structure on a reasonable time scale (see the equilibration of atomic deviations in Fig. S8, red line), at variance with what we have found for other large proteins [66,70,71]. Thus, the effect of high temperature was further tested by using the CABS-flex algorithm [51] for mimicking protein structure flexibility, which focuses on the coarse-grained modeling of large-scale conformational transitions. In particular, we used a temperature twice larger than that typically used to reproduce the native protein state, which is usually sufficient for the complete melting of unrestrained small polypeptide chains [52]. The results shown in Fig. 9 B indicate again a high flexibility for a large number of protein regions, scattered throughout the whole sequence. The fluctuations calculated by using the CABS-flex and MD data were generally in very good agreement (see regions highlighted in cyan both in Fig. 9 A and B, each consisting of at least 20 residues), although the former tended to be higher in some N-terminal protein regions (around residue 130 and 170), and the latter in some C-terminal ones (around position 610 and 630). In any case, no indication was found of the potential presence of an unfolding intermediate in the denaturation process. Furthermore, although the contact map of the protein residues (reported in Fig. S9) showed that most of the inner interactions in the homodimer took place within each monomer (and, for both monomers, predominantly within each of their three subdomains), no indication was found of the dissociation of the two monomers. This suggests that the overall secondary, tertiary and quaternary structure of PADI4 might not be lost at very different stages during the unfolding process.

4. Discussion

Under conditions of cellular stress, some proteins can undergo several processes of PTM, such as citrullination. The conversion of arginine residues to citrulline by PADI enzymes, results in the recognition by the immune system of the citrullinated proteins; this recognition occurs in cancer and other diseases. PADI proteins are mostly cytosolic; however, PADI4 has an NLS that allows its nuclear translocation, and therefore it can citrullinate nuclear targets such as histones. Our results not only indicate that the PADI4 gene is significantly expressed in various tumour types, but further show different protein expression levels and patterns. The WB analyses showed that different tumour cell lines had levels of PADI4 protein expression that ranged from very low in PAAD to high in COAD and GBM. Moreover, protein extracts revealed multiple PADI4 protein bands that reflected the fact that PADI4 could undergo alternative splicing, and then generate protein species with or without NLS, resulting in a different subcellular localization. Immunostaining with anti-PADI4 antibody confirmed: (i) the expression of PADI4 in the above-mentioned tumours; and (ii) its tumour-dependent distribution.

The p53 gene is considered the most frequent target of genetic alteration identified in human cancers [72]. Biological functions of p53 include: G1 arrest induction, apoptosis following DNA damage or other cellular insults, genomic stability maintenance, and angiogenesis inhibition. To perform those functions, p53 binds DNA in a sequence-specific fashion [73] resulting in a transcriptional activation of downstream genes that carry out a variety of functions. Biochemical assays indicate that p53 interacts with PADI4 both in cells and when the two are combined as purified proteins [24]. Our results show that tumour cell lines differed in the levels of certain PADI4 protein forms and p53 (Fig. 1 B). Since PADI4 plays a role during tumorigenesis by antagonizing regulation of p53 to tumour suppressor genes [54], we hypothesize that PADI4 might play a different role on the cell function and development depending on the tumour origin. These results are in line with the observations made on several types of cancers, where it has been highlighted the major role of PADI4 at the onset and progression of cancer [74]. Therefore, tampering with citrullination has been proposed as a possible target for developing cancer treatments [75].

Given the important role of PADI4 in cancer, we reasoned that a first step in deciphering its protein interactome and its function was to perform its biophysical and conformational characterization. The biophysical and biochemical features described in this work will also help to understand how PADI4 mediates its interactions and its regulation with putative therapeutic agents. We found that PADI4 in solution possessed a native structure in a narrow pH range, between 6.5 and 8.0. In such pH range, the ellipticity at 222 nm showed the highest value (in absolute terms) and we could observe sigmoidal thermal denaturations. The acquisition of native secondary and tertiary structure, as well as the burial of solvent-exposed hydrophobic surface, occurred concomitantly,

either starting from acidic or basic pH values. We could not explore the acquisition of native quaternary structure at low pH values, since the protein precipitated at the concentrations used in the DLS experiments. The fact that the protein species populated at low pH showed a large ANS binding suggests that they are probably molten globules [58], as we could further confirm by the absence of thermal unfolding sigmoidal curves in the fluorescence or CD experiments at low pH values (data not shown). The optimal activity for histone H3 citrullination is between pH 6.4 and 7.2 [76], close to the pH range observed for the acquisition of native secondary structure of PADI4. A similar pH range was observed for citrullination of the model compound N-α-benzoyl L-arginine ethyl ester [77]. Therefore, the pH range where PADI4 acquires a native conformation seems to be within its range for optimal activity. It has been shown that, due to the increased glucose metabolism, the production of H^+ is enhanced in cancer states, resulting in acidification of the extracellular milieu (in the range of pH from 6.5 to 6.9) and, in parallel, an alkalization of the cytoplasm environment (pH > 7.2) [78,79]. We hypothesize that even these variations of pH in cancer cells do not alter the functionality of PADI4. However, in such pH range (between 6.5 and 8.0) the apparent T_m values of the protein were ~55 °C. We are fully aware, that judging protein stability based only on the value of an apparent T_m can skew our reasoning (in fact, the use of T_m to judge protein stability can be properly used when comparing similar proteins, such as in the case of mutants). However, the apparent ΔG for PADI4 is ~4 kcal mol^{-1}, which is small for a 74 kDa protein; similar values of the apparent thermal denaturation midpoints have been observed for other large proteins [65,66], where they has been associated with a low stability, which often occurs in proteins with large flexibility. Our simulation results support this latter view, as they indicate the dynamics of the protein is almost uniformly distributed on the whole sequence, in spite of being formed by distinct subdomains.

PADI enzymes are activated by millimolar concentrations of Ca^{2+} which can occur, for instance, during apoptosis. Our *in vitro* analysis showed that the presence of Ca^{2+} did not alter the quaternary structure of the protein, and PADI4 remained dimeric in the presence of the cation (Fig. 5). However, the local environment around some of the tryptophans and/or tyrosines changed when the cation was present in solution (Fig. S1), and the use of a probe such as SYPRO Orange indicates differences in the solvent-exposure of hydrophobic patches in the protein in the Ca^{2+}-free species (Fig. S3). These findings agree with results found in the X-ray structure of PADI4 in the absence of Ca^{2+}, where the regions Ile313-Ile320, Pro338-Met348, Pro371-Pro387, Pro396-Gly403 and Phe633-His644 are solvent-exposed and highly disordered [80]. All these regions become well-ordered in the presence of the cation. Furthermore, the region from Glu351 to Ala359 has a conformational change and acquires a β-strand conformation in the presence of Ca^{2+}. It is interesting to note that Tyr356, Trp547 and Tyr636 are included in some of those regions, explaining the changes in the intrinsic fluorescence observed under the two conditions (Fig. S1) and the results of SYPRO Orange (Fig. S3). In addition, the presence of Ca^{2+} induced a considerable stabilization of PADI4, as observed by DSC, although the effect may be masked by a further irreversible stage during the denaturation process.

We also found that PADI4 had a complex unfolding behaviour, as shown by our DSC findings, in the presence of Ca^{2+} and during the chemical denaturations. The far-UV CD chemical denaturation curves used to explore the folding of PADI4 showed at least two intermediates, at variance with the chemical denaturations observed by fluorescence and the MD simulations. These findings indicate that the unfolding of PADI4 was not a two-state process [81]. Furthermore, the CD and ANS results suggest the presence of nearby solvent-exposed hydrophobic patches in the structure of the protein at physiological conditions, which are disrupted by low denaturant concentrations resulting in a step-by-step increase of the ellipticity in absolute value, and then in the helicity of the protein. The increase of the fluorescence of the ANS at low GdmCl concentrations, suggests that those hydrophobic patches are close enough among them in the native structure to bind the probe, and probably to some PADI4 partners. The simulation results also suggest that the protein regions with higher flexibility at room temperature are the same that show an enhanced dynamic during the first steps of the thermal unfolding process. Furthermore, the melting of the secondary structure does not seem to be accompanied by large scale conformational transitions, neither by the loss of the protein quaternary structure.

5. Conclusions

PADI proteins are present in a large number of cell and tissue types, and have an important role in key biochemical pathways. In this work, we have performed a comprehensive biophysical analysis of PADI4, by using a variety of techniques. The results have revealed aspects of the protein stability and dynamics that could have a significant importance in the interaction with various molecular partners, for instance, in the histones citrullination. Furthermore, our biochemical characterization, performed by using different cancer cell lines, indicated the presence of PADI4 in different subcellular localizations. Our observations also support a role of this protein in regulating the expression of p53. Taken all together, the results here presented not only agree with the proposed role of PADI4 in the onset and progression of cancer, but also set the knowledge for the development of tools to study the function of PADI4. .

Author contributions and competing interests

JLN, ACA, BR, AVC and CdJ designed the experiments and the research methodology. JLN, ACA, AMG, BR, OA and SAA carried out the experiments. JLN, ACA, AMG, BR, AVC, SAA and CdJ analysed the data. JLN, OA, AVC and CdJ provided funding acquisition and project administration. All authors wrote, revised, edited and corrected the manuscript.

Declaration of competing interest

The authors declare no competing interests.

Data availability

Data will be made available on request.

Funding and Acknowledgements

This work was supported by Spanish Ministry of Economy and Competitiveness and European ERDF Funds (MCIU/AEI/FEDER, EU) [RTI2018-097991-B-I00 to JLN, BFU2016-78232-P to AVC; CP19/00095 to CdJ]; Fondo de Investigaciones Sanitarias from Instituto de Salud Carlos III, and European Union (ERDF/ESF, "Investing in your future") [PI18/00349 to OA]; Diputación General de Aragón ["Protein targets and Bioactive Compounds group" E45-20R to AVC, and "Digestive Pathology Group" B25-20R to OA]. SAA was recipient of a "Carolina Foundation predoctoral fellowship" 2020. The funders had no role in the study design, data collection and analysis, decision to publish, or preparation of the manuscript.

We thank Dr. Miguel Saceda (IDIBE) for providing us with the tumour cell lines used in this work. We thank the two anonymous reviewers for helpful suggestions and discussions. BR acknowledges the kind use of computational resources by the European Magnetic Resonance Center (CERM), Sesto Fiorentino (Florence), Italy.

Appendix A. Supplementary data

Supplementary data to this article can be found online at https://doi.org/10.1016/j.abb.2022.109125.

References

[1] S. Mondal, P.R. Thompson, Protein arginine deiminases (PADs): Biochemistry and chemical biology of protein citrullination, Acc. Chem. Res. 52 (2019) 818–832, https://doi.org/10.1021/ACS.ACCOUNTS.9B00024.

[2] E.R. Vossenaar, A.J.W. Zendman, W.J. Van Venrooij, G.J.M. Pruijn, PAD, a growing family of citrullinating enzymes: genes, features and involvement in disease, Bioessays 25 (2003) 1106–1118, https://doi.org/10.1002/BIES.10357.

[3] G.L. Cuthbert, S. Daujat, A.W. Snowden, H. Erdjument-Bromage, T. Hagiwara, M. Yamada, R. Schneider, P.D. Gregory, P. Tempst, A.J. Bannister, T. Kouzarides, Histone deimination antagonizes arginine methylation, Cell 118 (2004) 545–553, https://doi.org/10.1016/J.CELL.2004.08.020.

[4] H. Asaga, M. Yamada, T. Senshu, Selective deimination of vimentin in calcium ionophore-induced apoptosis of mouse peritoneal macrophages, Biochem. Biophys. Res. Commun. 243 (1998) 641–646, https://doi.org/10.1006/BBRC.1998.8148.

[5] C. Assohou-Luty, R. Raijmakers, W.E. Benckhuijsen, J. Stammen-Vogelzangs, A. De Ru, P.A. Van Veelen, K.L.M.C. Franken, J.W. Drijfhout, G.J.M. Pruijn, The human peptidylarginine deiminases type 2 and type 4 have distinct substrate specificities, Biochim. Biophys. Acta 1844 (2014) 829–836, https://doi.org/10.1016/J.BBAPAP.2014.02.019.

[6] T. Senshu, K. Akiyama, A. Ishigami, K. Nomura, Studies on specificity of peptidylarginine deiminase reactions using an immunochemical probe that recognizes an enzymatically deiminated partial sequence of mouse keratin K1, J. Dermatol. Sci. 21 (1999) 113–126, https://doi.org/10.1016/S0923-1811(99)00026-2.

[7] K. Kizawa, H. Takahara, H. Troxler, P. Kleinert, U. Mochida, C.W. Heizmann, Specific citrullination causes assembly of a globular S100A3 homotetramer: a putative Ca^{2+} modulator matures human hair cuticle, J. Biol. Chem. 283 (2008) 5004–5013, https://doi.org/10.1074/JBC.M709357200/ATTACHMENT/30FDC955-973C-47BA-B803-D6787A3A216D/MMC1.PDF.

[8] Y. Wang, J. Wysocka, J. Sayegh, Y.H. Lee, J.R. Pertin, L. Leonelli, L.S. Sonbuchner, C.H. McDonald, R.G. Cook, Y. Dou, R.G. Roeder, S. Clarke, M.R. Stallcup, C.D. Allis, S.A. Coonrod, Human PAD4 regulates histone arginine methylation levels via demethylimination, Science 306 (2004) 279–283, https://doi.org/10.1126/SCIENCE.1101400/SUPPL_FILE/WANG.SOM.PDF.

[9] A. Ishigami, N. Maruyama, Importance of research on peptidylarginine deiminase and citrullinated proteins in age-related disease, Geriatr. Gerontol. Int. 10 (2010) S53–S58, https://doi.org/10.1111/J.1447-0594.2010.00593.X.

[10] R.J. Klose, Y. Zhang, Regulation of histone methylation by demethylimination and demethylation, Nat. Rev. Mol. Cell Biol. 8 (2007) 307–318, https://doi.org/10.1038/nrm2143.

[11] B. György, E. Tóth, E. Tarcsa, A. Falus, E.I. Buzás, Citrullination: a posttranslational modification in health and disease, Int. J. Biochem. Cell Biol. 38 (2006) 1662–1677, https://doi.org/10.1016/J.BIOCEL.2006.03.008.

[12] C. Anzilotti, F. Pratesi, C. Tommasi, P. Migliorini, Peptidylarginine deiminase 4 and citrullination in health and disease, Autoimmun. Rev. 9 (2010) 158–160, https://doi.org/10.1016/J.AUTREV.2009.06.002.

[13] L.L. Wang, Y.P. Song, J.H. Mi, M.L. Ding, Peptidyl arginine deiminase 4 and its potential role in Alzheimer's disease, Med. Hypotheses 146 (2021) 110466, https://doi.org/10.1016/J.MEHY.2020.110466.

[14] M. Guerrin, A. Ishigami, M.C. Méchin, R. Nachat, S. Valmary, M. Sebbag, M. Simon, T. Senshu, G. Serre, cDNA cloning, gene organization and expression analysis of human peptidylarginine deiminase type I, Biochem. J. 370 (2003) 174, https://doi.org/10.1042/BJ20020870.

[15] A. Ishigami, T. Ohsawa, H. Asaga, K. Akiyama, M. Kuramoto, N. Maruyama, Human peptidylarginine deiminase type II: molecular cloning, gene organization, and expression in human skin, Arch. Biochem. Biophys. 407 (2002) 25–31, https://doi.org/10.1016/S0003-9861(02)00516-7.

[16] T. Kanno, A. Kawada, J. Yamanouchi, C. Yosida-Noro, A. Yoshiki, M. Shiraiwa, M. Kusakabe, M. Manabe, T. Tezuka, H. Takahara, Human peptidylarginine deiminase type III: molecular cloning and nucleotide sequence of the cDNA, properties of the recombinant enzyme, and immunohistochemical localization in human skin, J. Invest. Dermatol. 115 (2000) 813–823, https://doi.org/10.1046/J.1523-1747.2000.00131.X.

[17] S. Chavanas, M.C. Méchin, H. Takahara, A. Kawada, R. Nachat, G. Serre, M. Simon, Comparative analysis of the mouse and human peptidylarginine deiminase gene clusters reveals highly conserved non-coding segments and a new human gene, PADI6, Gene 330 (2004) 19–27, https://doi.org/10.1016/J.GENE.2003.12.038.

[18] K. Nakashima, T. Hagiwara, A. Ishigami, S. Nagata, H. Asaga, M. Kuramotot, T. Senshu, M. Yamada, Molecular characterization of peptidylarginine deiminase in HL-60 cells induced by retinoic acid and 1α,25-dihydroxyvitamin D3, J. Biol. Chem. 274 (1999) 27786–27792, https://doi.org/10.1074/JBC.274.39.27786.

[19] S. Dong, T. Kanno, A. Yamaki, T. Kojima, M. Shiraiwa, A. Kawada, M.C. Méchin, S. Chavanas, G. Serre, M. Simon, H. Takahara, NF-Y and Sp1/Sp3 are involved in the transcriptional regulation of the peptidylarginine deiminase type III gene (PADI3) in human keratinocytes, Biochem. J. 397 (2006) 449–459, https://doi.org/10.1042/BJ20051939.

[20] S. Chavanas, V. Adoue, M.C. Méchin, S. Ying, S. Dong, H. Duplan, M. Charveron, H. Takahara, G. Serre, M. Simon, Long-range enhancer associated with chromatin looping allows AP-1 regulation of the peptidylarginine deiminase 3 gene in differentiated keratinocyte, PLoS One 3 (2008), e3408, https://doi.org/10.1371/JOURNAL.PONE.0003408.

[21] M.C. Méchin, M. Enji, R. Nachat, S. Chavanas, M. Charveron, A. Ishida-Yamamoto, G. Serre, H. Takahara, M. Simon, The peptidylarginine deiminases expressed in human epidermis differ in their substrate specificities and subcellular locations, Cell. Mol. Life Sci. 62 (2005) 1984–1995, https://doi.org/10.1007/S00018-005-5196-Y.

[22] K.P. U, V. Subramanian, A.P. Nicholas, P.R. Thompson, P. Ferretti, Modulation of calcium-induced cell death in human neural stem cells by the novel peptidylarginine deiminase–AIF pathway, Biochim. Biophys. Acta 1843 (2014) 1162–1171, https://doi.org/10.1016/J.BBAMCR.2014.02.018.

[23] H.C. Hung, C.Y. Lin, Y.F. Liao, P.C. Hsu, G.J. Tsay, G.Y. Liu, The functional haplotype of peptidylarginine deiminase IV (S55G, A82V and A112G) associated with susceptibility to rheumatoid arthritis dominates apoptosis of acute T leukemia Jurkat cells, Apoptosis 12 (2007) 475–487, https://doi.org/10.1007/S10495-006-0005-0/FIGURES/7.

[24] P. Li, H. Yao, Z. Zhang, M. Li, Y. Luo, P.R. Thompson, D.S. Gilmour, Y. Wang, Regulation of p53 target gene expression by peptidylarginine deiminase 4, Mol. Cell Biol. 28 (2008) 4745–4758, https://doi.org/10.1128/MCB.01747-07.

[25] P. Li, D. Wang, H. Yao, P. Doret, G. Hao, Q. Shen, H. Qiu, X. Zhang, Y. Wang, G. Chen, Y. Wang, Coordination of PAD4 and HDAC2 in the regulation of p53-target gene expression, Oncogene 29 (2010) 3153–3162, https://doi.org/10.1038/onc.2010.51.

[26] K. Nakashima, T. Hagiwara, M. Yamada, Nuclear localization of peptidylarginine deiminase V and histone deimination in granulocytes, J. Biol. Chem. 277 (2002) 49562–49568, https://doi.org/10.1074/JBC.M208795200.

[27] J.E. Jones, C.P. Causey, B. Knuckley, J.L. Slack-Noyes, P.R. Thompson, Protein arginine deiminase 4 (PAD4): current understanding and future therapeutic potential, Curr. Opin. Drug Discov. Dev 12 (2009) 627.

[28] D. Chen, M. Ma, H. Hong, S.S. Koh, S.M. Huang, B.T. Schurter, D.W. Aswad, M. R. Stallcup, Regulation of transcription by a protein methyltransferase, Science 284 (1999) 2174–2177, https://doi.org/10.1126/science.284.5423.2174.

[29] K. Funabashi, M. Sawata, A. Nagai, M. Akimoto, R. Mashimo, H. Takahara, K. Kizawa, P.R. Thompson, K. Ite, K. Kitanishi, M. Unno, Structures of human peptidylarginine deiminase type III provide insights into substrate recognition and inhibitor design, Arch. Biochem. Biophys. 708 (2021) 108911, https://doi.org/10.1016/J.ABB.2021.108911.

[30] O. Rechiche, T. Verne Lee, J. Shaun Lott, Structural characterization of human peptidyl-arginine deiminase type III by X-ray crystallography, Acta Crystallogr. F77 (2021) 334–340, https://doi.org/10.1107/S2053230X21009195.

[31] N. Horikoshi, H. Tachiwana, K. Saito, A. Osakabe, M. Sato, M. Yamada, S. Akashi, Y. Nishimura, W. Kagawa, H. Kurumizaka, Structural and biochemical analyses of the human PAD4 variant encoded by a functional haplotype gene, Acta Crystallogr. D67 (2011) 112–118, https://doi.org/10.1107/S0907444910051711.

[32] S.C. Gill, P.H. von Hippel, Calculation of protein extinction coefficients from amino acid sequence data, Anal. Biochem. 182 (1989) 319–326, https://doi.org/10.1016/0003-2697(89)90602-7.

[33] M. Fuentes-Baile, D. Bello-Gil, E. Pérez-Valenciano, J.M. Sanz, P. García-Morales, B. Maestro, M.P. Ventero, C. Alenda, V.M. Barberá, M. Saceda, CLyta-DAAO, free and immobilized in magnetic nanoparticles, induces cell death in human cancer cells, Biomolecules 10 (2020) 222, https://doi.org/10.3390/biom10020222.

[34] M.P. Ventero, M. Fuentes-Baile, C. Quereda, E. Perez-Valeciano, C. Alenda, P. Garcia-Morales, D. Esposito, P. Dorado, V.M. Barbera, M. Saceda, Radiotherapy resistance acquisition in glioblastoma. Role of SOCS1 and SOCS3, PLoS One 14 (2019), e0212581, https://doi.org/10.1371/journal.pone.0212581.

[35] Y. Nozaki, The preparation of guanidine hydrochloride, Methods Enzymol. 26 (1972) 43–50, https://doi.org/10.1016/S0076-6879(72)26005-0.

[36] P. Cimmperman, D. Matulis, Protein thermal denaturation measurements via a fluorescent dye, in: A. Podjrany, A. Dejaegere, B. Kieffer (Eds.), Biophysical Approaches Determining Ligand Binding to Biomolecular Targets: Detection, Measurement and Modelling, Royal Society of Chemistry, London, 2011, pp. 247–274, https://doi.org/10.1039/9781849732666-00247.

[37] A. Velazquez-Campoy, J. Sancho, O. Abian, S. Vega, Biophysical screening for identifying pharmacological chaperones and inhibitors against conformational and infectious diseases, Curr. Drug Targets 17 (2016) 1492–1505, https://doi.org/10.2174/1389450117666160201110449.

[38] S. Benjwal, S. Verma, K.-H. Röhm, O. Gursky, Monitoring protein aggregation during thermal unfolding in circular dichroism experiments, Protein Sci. 15 (2006) 635–639, https://doi.org/10.1110/PS.051917406.

[39] C.A. Royer, Fluorescence spectroscopy, in: N. Shirley (Ed.), Protein Stability and Folding, Humana Press, Totowa, NJ, 1995, pp. 65–89, https://doi.org/10.1385/0-89603-301-5:65.

[40] C.M. Doyle, J.A. Rumfeldt, H.R. Broom, A. Broom, P.B. Stathopulos, K.A. Vassall, J. J. Almey, E.M. Meiering, Energetics of oligomeric protein folding and association, Arch. Biochem. Biophys. 531 (2013) 44–64, https://doi.org/10.1016/J.ABB.2012.12.005.

[41] L.M. Gloss, Equilibrium and kinetic approaches for studying oligomeric protein folding, Methods Enzymol. 466 (2009) 325–357, https://doi.org/10.1016/S0076-6879(09)66014-6.

[42] J. Backmann, G. Schäfer, L. Wyns, H. Bönisch, Thermodynamics and kinetics of unfolding of the thermostable trimeric adenylate kinase from the archaeon *Sulfolobus acidocaldarius*, J. Mol. Biol. 284 (1998) 817–833, https://doi.org/10.1006/JMBI.1998.2216.

[43] J.L. Neira, F. Hornos, J. Bacarizo, A. Cámara-Artigás, J. Gómez, The monomeric species of the regulatory domain of tyrosine hydroxylase has a low conformational stability, Biochemistry 55 (2016) 3418–3431, https://doi.org/10.1021/ACS.BIOCHEM.6B00135/SUPPL_FILE/BI6B00135_SI_001.PDF.

[44] A. Šali, T.L. Blundell, Comparative protein modelling by satisfaction of spatial restraints, J. Mol. Biol. 234 (1993) 779–815, https://doi.org/10.1006/JMBI.1993.1626.

[45] M.J. Abraham, T. Murtola, R. Schulz, S. Páll, J.C. Smith, B. Hess, E. Lindah, GROMACS: high performance molecular simulations through multi-level parallelism from laptops to supercomputers, Software 1–2 (2015) 19–25, https://doi.org/10.1016/J.SOFTX.2015.06.001.
[46] K. Lindorff-Larsen, S. Piana, K. Palmo, P. Maragakis, J.L. Klepeis, R.O. Dror, D. E. Shaw, Improved side-chain torsion potentials for the Amber ff99SB protein force field, Proteins Struct. Funct. Bioinforma. 78 (2010) 1950–1958, https://doi.org/10.1002/PROT.22711.
[47] W.L. Jorgensen, J. Chandrasekhar, J.D. Madura, R.W. Impey, M.L. Klein, Comparison of simple potential functions for simulating liquid water, J. Chem. Phys. 79 (1998) 926, https://doi.org/10.1063/1.445869.
[48] J.L. Neira, B. Rizzuti, J.L. Iovanna, Determinants of the pKa values of ionizable residues in an intrinsically disordered protein, Arch. Biochem. Biophys. 598 (2016) 18–27, https://doi.org/10.1016/J.ABB.2016.03.034.
[49] S. Evoli, R. Guzzi, B. Rizzuti, Molecular simulations of β-lactoglobulin complexed with fatty acids reveal the structural basis of ligand affinity to internal and possible external binding sites, Proteins Struct. Funct. Bioinforma. 82 (2014) 2609–2619, https://doi.org/10.1002/PROT.24625.
[50] B. Rizzuti, V. Daggett, Using simulations to provide the framework for experimental protein folding studies, Arch. Biochem. Biophys. 531 (2013) 128–135, https://doi.org/10.1016/J.ABB.2012.12.015.
[51] M. Jamroz, M. Orozco, A. Kolinski, S. Kmiecik, Consistent view of protein fluctuations from all-atom molecular dynamics and coarse-grained dynamics with knowledge-based force-field, J. Chem. Theor. Comput. 9 (2013) 119–125, https://doi.org/10.1021/CT300854W/SUPPL_FILE/CT300854W_SI_002.PDF.
[52] A. Kuriata, A.M. Gierut, T. Oleniecki, M.P. Ciemny, A. Kolinski, M. Kurcinski, S. Kmiecik, CABS-flex 2.0: a web server for fast simulations of flexibility of protein structures, Nucleic Acids Res. 46 (2018) W338–W343, https://doi.org/10.1093/NAR/GKY356.
[53] X. Chang, J. Han, Expression of peptidylarginine deiminase type 4 (PAD4) in various tumors, Mol. Carcinog. 45 (2006) 183–196, https://doi.org/10.1002/MC.20169.
[54] X. Chang, J. Han, L. Pang, Y. Zhao, Y. Yang, Z. Shen, Increased PADI4 expression in blood and tissues of patients with malignant tumors, BMC Cancer 9 (2009) 40, https://doi.org/10.1186/1471-2407-9-40.
[55] N. Moshkovich, H.J. Ochoa, B. Tang, H.H. Yang, Y. Yang, J. Huang, M.P. Lee, L. M. Wakefield, Peptidylarginine deiminase IV regulates breast cancer stem cells via a novel tumor cell-autonomous suppressor role, Cancer Res. 80 (2020) 2125–2137, https://doi.org/10.1158/0008-5472.CAN-19-3018.
[56] O. Laptenko, C. Prives, Transcriptional regulation by p53: one protein, many possibilities, Cell Death Differ. 13 (2006) 951–961, https://doi.org/10.1038/SJ.CDD.4401916.
[57] B. Vogelstein, D. Lane, A.J. Levine, Surfing the p53 network, Nature 408 (2000) 307–310, https://doi.org/10.1038/35042675.
[58] O.B. Ptitsyn, Molten globule and protein folding, Adv. Protein Chem. 47 (1995) 83–229, https://doi.org/10.1016/S0065-3233(08)60546-X.
[59] Y.-H. Chen, J.T. Yang, K.H. Chau, Determination of the helix and β form of proteins in aqueous solution by circular dichroism, Biochemistry 13 (2002) 3350–3359, https://doi.org/10.1021/BI00713A027.
[60] S. Vuilleumier, J. Sancho, R. Loewenthal, A.R. Fersht, Circular dichroism studies of barnase and its mutants: characterization of the contribution of aromatic side chains, Biochemistry 32 (1993) 10303–10313.
[61] S.M. Kelly, T.J. Jess, N.C. Price, How to study proteins by circular dichroism, Biochim. Biophys. Acta Protein Proteonomics 1751 (2005) 119–139, https://doi.org/10.1016/J.BBAPAP.2005.06.005.
[62] S. Kelly, N. Price, The use of circular dichroism in the investigation of protein structure and function, Curr. Protein Pept. Sci. 1 (2000) 349–384, https://doi.org/10.2174/1389203003381315.
[63] R.W. Woody, Circular dichroism, Methods Enzymol. 246 (1995) 34–71, https://doi.org/10.1016/0076-6879(95)46006-3.
[64] J.L. Neira, S. Vega, S. Martínez-Rodríguez, A. Velázquez-Campoy, The isolated GTPase-activating-protein-related domain of neurofibromin-1 has a low conformational stability in solution, Arch. Biochem. Biophys. 700 (2021) 108767, https://doi.org/10.1016/J.ABB.2021.108767.
[65] A.M. Giudici, J.G. Hernández-Cifre, A. Cámara-Artigas, F. Hornos, S. Martínez-Rodríguez, J. Carlos Alvarez-Pérez, I. Díaz-Cano, M. Esther Fárez-Vidal, J.L. Neira, The isolated armadillo-repeat domain of Plakophilin 1 is a monomer in solution with a low conformational stability, J. Struct. Biol. 211 (2020) 107569, https://doi.org/10.1016/J.JSB.2020.107569.
[66] C. Díaz-García, F. Hornos, A.M. Giudici, A. Cámara-Artigas, J.R. Luque-Ortega, A. Arbe, B. Rizzuti, C. Alfonso, J.K. Forwood, J.L. Iovanna, J. Gómez, M. Prieto, A. Coutinho, J.L. Neira, Human importin α3 and its N-terminal truncated form, without the importin-β-binding domain, are oligomeric species with a low conformational stability in solution, Biochim. Biophys. Acta Gen. Subj. 1864 (2020) 129609, https://doi.org/10.1016/J.BBAGEN.2020.129609.
[67] Y.L. Liu, Y.H. Chiang, G.Y. Liu, H.C. Hung, Functional role of dimerization of human peptidylarginine deiminase 4 (PAD4), PLoS One 6 (2011), e21314, https://doi.org/10.1371/JOURNAL.PONE.0021314.
[68] R. Day, B.J. Bennion, S. Ham, V. Daggett, Increasing temperature accelerates protein unfolding without changing the pathway of unfolding, J. Mol. Biol. 322 (2002) 189–203, https://doi.org/10.1016/S0022-2836(02)00672-1.
[69] B. Rizzuti, V. Daggett, R. Guzzi, L. Sportelli, The early steps in the unfolding of azurin, Biochemistry 43 (2004) 15604–15609, https://doi.org/10.1021/BI048685T.
[70] L.M. Contreras, P. Sevilla, A. Cámara-Artigas, J.G. Hernández-Cifre, B. Rizzuti, F. J. Florencio, M.I. Muro-Pastor, J.G. de la Torre, J.L. Neira, The cyanobacterial ribosomal-associated protein LrtA from Synechocystis sp. PCC 6803 is an oligomeric protein in solution with chameleonic sequence properties, Int. J. Mol. Sci. 19 (2018) 1857, https://doi.org/10.3390/IJMS19071857.
[71] A. Guglielmelli, B. Rizzuti, R. Guzzi, Stereoselective and domain-specific effects of ibuprofen on the thermal stability of human serum albumin, Eur. J. Pharmaceut. Sci. 112 (2018) 122–131, https://doi.org/10.1016/J.EJPS.2017.11.013.
[72] M. Hollstein, D. Sidransky, B. Vogelstein, C.C. Harris, p53 mutations in human cancers, Science 253 (1991) 49–53, https://doi.org/10.1126/SCIENCE.1905840.
[73] S.E. Kern, J.A. Pietenpol, S. Thiagalingam, A. Seymour, K.W. Kinzler, B. Vogelstein, Oncogenic forms of p53 inhibit p53-regulated gene expression, Science 256 (1992) 827–830, https://doi.org/10.1126/SCIENCE.1589764.
[74] N. Moshkovich, H.J. Ochoa, B. Tang, H.H. Yang, Y. Yang, J. Huang, M.P. Lee, L. M. Wakefield, Peptidylarginine Deiminase IV regulates breast cancer stem cells via a novel tumor cell-autonomous suppressor role, Cancer Res. 80 (2020) 2125–2137. https://doi.org/10.1158/0008-5472.
[75] V.A. Brentville, M. Vankemmelbeke, R.L. Metheringham, L.G. Durrant, Post-translational modifications such as citrullination are excellent targets for cancer therapy, Semin. Immunol. 47 (2020) 101393. https://doi.org/10.1016/j.smim.2020.101393.
[76] Y. Zhou, N. Mittereder, G.P. Sims, Perspective on protein arginine deiminase activity—Bicarbonate is a pH-independent regulator of citrullination, Front. Immunol. 9 (2018), https://doi.org/10.3389/FIMMU.2018.00034.
[77] B. Knuckley, M. Bhatia, P.R. Thompson, Protein arginine deiminase 4: evidence for a reverse protonation mechanism, Biochemistry 46 (2007) 6578–6587. https://doi.org/10.1021/bi700095s.
[78] E. Persi, M. Duran-Frigola, M. Damaghi, W.R. Roush, P. Aloy, J.L. Cleveland, R. J. Gillies, E. Ruppin, Systems analysis of intracellular pH vulnerabilities for cancer therapy, Nat. Commun. 9 (2018) 1–11, https://doi.org/10.1038/s41467-018-05261-x.
[79] V. Estrella, T. Chen, M. Lloyd, J. Wojtkowiak, H.H. Cornnell, A. Ibrahim-Hashim, K. Bailey, Y. Balagurunathan, J.M. Rothberg, B.F. Sloane, J. Johnson, R. A. Gatenby, R.J. Gillies, Acidity generated by the tumor microenvironment drives local invasion, Cancer Res. 73 (2013) 1524–1535, https://doi.org/10.1158/0008-5472.CAN-12-2796.
[80] K. Arita, H. Hashimoto, T. Shimizu, K. Nakashima, M. Yamada, M. Sato, Structural basis for Ca^{2+}-induced activation of human PAD4, Nat. Struct. Mol. Biol. 11 (2004) 777–783, https://doi.org/10.1038/nsmb799.
[81] S.E. Jackson, How do small single-domain proteins fold? Folding Des. 3 (1998) R81–R91, https://doi.org/10.1016/S1359-0278(98)00033-9.